Supplementary information

Impact of the surface microenvironment on the redox properties of a Co-based molecular cathode for selective aqueous electrochemical CO_2-to-CO reduction

Matthieu Haake,[1] Dmitry Aldakov,[2] Julien Pérard,[1] Giulia Veronesi,[1] Antonio Aguilar Tapia,[3] Bertrand Reuillard[1]* and Vincent Artero[1]

[1]Univ. Grenoble Alpes, CNRS, CEA, IRIG, Laboratoire de Chimie et Biologie des Métaux, 17 rue des Martyrs, F-38054 Grenoble, Cedex, France

[2]Univ. Grenoble Alpes, CNRS, CEA, Grenoble INP, IRIG, SyMMES, 17 rue des Martyrs, F-38000 Grenoble, France

[3] Institut de Chimie Moléculaire de Grenoble, UAR2607 CNRS Université Grenoble Alpes, Grenoble F-38000 (France)

Table des matières

Experimental section 2
Materials and reagents 2
Equipment 2
Synthesis 3
1. 1-(4-Bromobutyl)pyrene 3
2. 1-(4-Azidobutyl)pyrene 3
3. 4-(Pyren-1-yl)butyl-1-amine 4
4. (4-Chloropyridine-2,6-diyl)bis(morpholinomethanone) (2) 5
5. 4-Chloro-2,6-diacetylpyridine (3) 5
6. Tert-butyl 4-(2,6-diacetylpyridin-4-yl)benzoate (4) 6
7. $[Co^{III}(N_4^{COOtBu})Cl_2]Cl$ (5) 6
8. $[Co^{III}(N_4^{COOH})Cl_2]Cl$ (6) 7
9. $[Co^{III}(N_4^{Bu\text{-}Pyr})Cl_2]Cl$ (**$CoN_4H\text{-}Ph_{Pyr}$**) 7
10. $[Co^{III}(N_4^{Bu})Cl_2]Cl$ (**$CoN_4H\text{-}Ph_{Bu}$**) 9
$CoN_4H\text{-}Ph_{Pyr}$|MWCNTs electrode preparation 9
Electrochemistry 10
XPS 10
Operando XAS spectroscopy measurements 11
EXAFS data treatment and analysis 12

Inductively coupled plasma atomic emission spectroscopy (ICP-AES) 13
Calculation of $K_{CoN4H\text{-}PhPyr}$ using a fitted Langmuir isotherm 14
Product quantification..... 15
FE, TONs and TOFs calculations..... 15
Treatment of Data 16
Supporting table and figures 17
References..... 36

Experimental section

Materials and reagents

CBr_4 and $CoCl_2 \cdot 6\ H_2O$ were purchased from Acros Organics and chelidamic acid monohydrate was purchased from TCI. All other used chemicals were purchased from Sigma–Aldrich. All chemicals were used without further purification unless overwise stated. Hydrogen gas was produced using a *FDGSi* hydrogen generator. Multi-walled carbon nanotubes (MWCNT) NC7000™ series were purchased from NANOCYL® and used without further purifications. For electrochemical analysis, 99.98% anhydrous acetonitrile (extra dry over molecular sieves) was used. Milli-Q water was obtained through a Millipore system (18.2 MΩ·cm). CO_2 gas extra pure was purchased from Air Products and used without additional purification. The parent complex **CoN_4H** was synthesized following previously reported literature.[1]

Equipment

^1H NMR experiments were carried out with a Bruker Advance 300 MHz or 400 MHz. ^{13}C NMR spectra were obtained with a Bruker Advance 400 MHz. IR spectra were recorded with a PerkinElmer Spectrum spectrometer. Mass spectrometry was performed on a Thermo Scientific LXQ mass spectrometer equipped with an electrospray source at the Service de Chimie Inorganique et Bioinorganique of CEA-Grenoble/CNRS. High-resolution mass spectra (HRMS) were performed on a Bruker maXis mass spectrometer by the SALSA platform from ICOA laboratory. UV-vis spectra were recorded with a Cary 60 UV-vis spectrometer. ICP-OES measurements were carried out with a Shimadzu ICPE-9000 from the IRIG-DIESE-LCBM laboratory following an eight-point calibration. XPS spectra were obtained with a Versa Probe II spectrometer (ULVAC- PHI) equipped with a monochromated Al K_α source (hv = 1486.6 eV). Cobalt K-edge X-ray Absorption Spectroscopy (XAS) analysis was performed at the CRG-FAME beamline (BM30) of the European Synchrotron Radiation Facility (ESRF, Grenoble, France).

Synthesis

1. 1-(4-Bromobutyl)pyrene

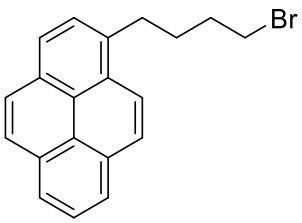

1-(4-bromobutyl)pyrene was synthesised following a previously described procedure.[2]

Tetrabromomethane (1.693 g, 5.11 mmol, 1.4 eq.) and triphenylphosphine (1.339 g, 5.11 mmol, 1.4 eq.) were added under argon atmosphere to a solution of 1-pyrenebutanol (1.020 g, 3.72 mmol, 1 eq.) in anhydrous THF (25 mL) cooled in an ice bath. As a white solid started to form the reaction mixture was allowed to reach room temperature by removing the ice bath. Then, the reaction mixture was stirred under argon atmosphere for another 16 h. The solution was then filtered over celite and the solvent was evaporated under reduced pressure. The crude residue was then purified by column chromatography over silica gel. As eluent, pure hexane followed by a hexane : DCM (80:20) mixture were used. The pure product (991 mg, 29.4 mmol, 79 %) was isolated as a white volatile solid.

^{1}H NMR (300 MHz, $CDCl_3$): δ = 8.27 (d, *J* = 9.3 Hz, 1H), 8.17 (dq, *J* = 7.9, 1.2 Hz, 2H), 8.12 (d, *J* = 8.4 Hz, 2H), 8.07 – 7.94 (m, 3H), 7.86 (d, *J* = 7.8 Hz, 1H), 3.53 – 3.41 (m, 2H), 3.45 – 3.32 (m, 2H), 2.04 (p, *J* = 3.6 Hz, 4H).

^{13}C NMR (75 MHz, $CDCl_3$): δ = 136.21 , 131.60 , 131.05 , 130.09 , 128.79 , 127.64 , 127.51 , 127.35 , 126.84 , 126.00 , 125.28 , 125.18 , 125.08 , 124.97 , 124.90 , 123.38 , 33.70 , 32.80 , 32.75 , 30.38 .

2. 1-(4-Azidobutyl)pyrene

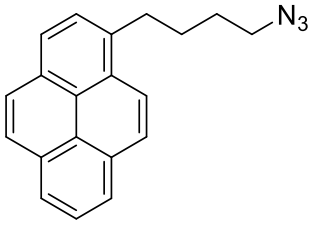

To a solution of 1-(4-bromobutyl)pyrene (503 mg, 1.48 mmol, 1 eq.) in DMF (10 mL) sodium azide (192 mg, 2.96 mmol, 2 eq.) was added under stirring. The reaction mixture was stirred for 16 h at 60 °C. Afterwards the reaction mixture was diluted with DCM (20 mL) and quenched with water (5 mL). The organic phase was collected and washed with water (2 x 4 mL) and concentrated sodium chloride

solution (2 x 4 mL). The organic phase was concentrated under reduced pressure. The residue was recrystallized from Et_2O. The pure product (397 mg, 1.32 mmol, 89 %) was obtained as a colorless crystalline needles.

^{1}H NMR (300 MHz, $CDCl_3$): δ = 8.26 (d, *J* = 9.3 Hz, 1H), 8.20 – 8.15 (m, 2H), 8.13 (s, 1H), 8.10 (d, *J* = 1.1 Hz, 1H), 8.05 – 7.97 (m, 3H), 7.86 (d, *J* = 7.8 Hz, 1H), 3.43 – 3.27 (m, 4H), 2.04 – 1.86 (m, 2H), 1.84 – 1.71 (m, 2H).

^{13}C NMR (75 MHz, $CDCl_3$): δ = 136.21 , 131.59 , 131.04 , 130.07 , 128.76 , 127.63 , 127.50 , 127.32 , 126.82, 125.99, 125.27, 125.17, 125.08, 124.95, 124.89, 123.34, 51.54 , 33.11 , 29.03, 28.96.

IR (ATR): $\tilde{\nu}$ (cm^{-1}) = 2092 (s, N_3).

3. 4-(Pyren-1-yl)butyl-1-amine

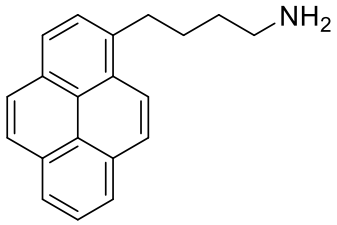

Pd/C (10 w%, 8.1 mg) was added to a solution of 1-(4-azidobutyl)pyrene (81.3 mg, 0.272 mmol, 1 eq.) in dry THF. Hydrogen was bubbled through the solution for 10 min leaving a hydrogen atmosphere over the reaction mixture. The reaction mixture was then stirred overnight at room temperature. The resulting suspension was filtered and the solvent was evaporated under reduced pressure. The pure product was obtained as a white-yellow oil (60.6 mg, 0.222 mmol, 82 %).

^{1}H NMR (300 MHz, $CDCl_3$): δ = 8.28 (d, *J* = 9.3 Hz, 1H), 8.16 (dq, *J* = 7.9, 1.2 Hz, 2H), 8.12 (d, *J* = 1.8 Hz, 1H), 8.09 (d, *J* = 3.3 Hz, 1H), 8.04 – 7.94 (m, 3H), 7.87 (d, *J* = 7.8 Hz, 1H), 3.40 – 3.32 (m, 2H), 2.76 (t, *J* = 7.1 Hz, 2H), 1.90 (tt, *J* = 9.3, 6.8 Hz, 2H), 1.70 – 1.56 (m, 2H), 1.39 (s, 2H).

^{13}C NMR (75 MHz, $CDCl_3$): δ = 136.90, 136.46, 131.55, 131.02, 129.89, 127.61, 127.32, 127.29, 126.65, 125.88, 125.20, 125.15, 124.93, 124.88, 124.76, 123.48, 42.24, 33.93, 33.45, 29.23.

IR (ATR): $\tilde{\nu}$ (cm^{-1}) = 3039 (s, N–H), 2932 (s, N–H), 2859 (s, N–H).

UV/vis: λ (nm) = 265 (ε = 4438 L mol^{-1} cm^{-3}), 277 (ε = 6430 L mol^{-1} cm^{-3}), 328 (ε = 4154 L mol^{-1} cm^{-3}), 344 (ε = 4824 L mol^{-1} cm^{-3}).

MS (ESI+, MeCN): m/z = 274.2 (100% $[M+H]^+$).

4. (4-Chloropyridine-2,6-diyl)bis(morpholinomethanone) (2)

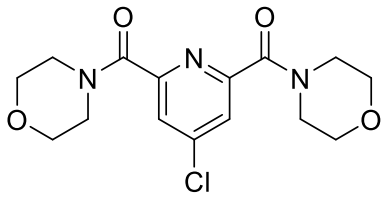

$SOCl_2$ (20 mL) was added to a solution of chelidamic acid monohydrate (4.0 g, 19.9 mmol, 1 eq.) in dry DMF (0.6 mL, 7.80 mmol, 0.4 eq.) at 0°C. The reaction mixture was then heated to reflux overnight under argon. Then, the solvent was removed under reduced pressure and a white solid was obtained. The crude product was dissolved in dry DCM (40 mL) and a 7.6 mL solution of morpholine (87.4 mmol, 4.4 eq.) in dry DCM was added dropwise at 0 °C. The reaction mixture was further stirred for 2 hours at room temperature. The solvent was then removed under reduced pressure, aqueous saturated $NaHCO_3$ solution (20 mL) was added and the product was extracted with ethyl acetate and washed with brine and water. The organic phase was dried over $MgSO_4$ and the solvent was evaporated under reduced pressure. The pure product was obtained as a white solid (6.09 mg, 17.91 mmol, 90 %).

^{1}H NMR (300 MHz, $CDCl_3$): δ = 7.72 (s, 2H), 3.78 (br, 8H), 3.66 – 3.62 (m, 8H).

^{13}C NMR (75 MHz, $CDCl_3$): δ = 165.55, 153.60, 146.83, 125.61, 67.01, 66.85, 47.81, 43.01.

5. 4-Chloro-2,6-diacetylpyridine (3)

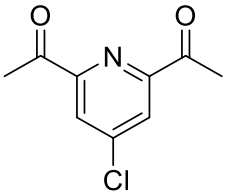

(4-chloropyridine-2,6-diyl)bis(morpholinomethanone) (1.4 g, 4.12 mmol, 1 eq.) was dissolved in dry freshly distilled THF (50 mL), under Argon. A 3 M MeMgCl solution in dry THF (3.43 mL, 10.3 mmol, 2.5 eq.) was then added dropwise at 0 °C. The reaction mixture was stirred for another 2 hours at room temperature, under argon, before being quenched with a saturated aqueous solution of NH_4Cl (50 mL) and then extracted with DCM. The organic phase was dried over $MgSO_4$ and the solvent was then evaporated under reduced pressure. The crude product was purified by column chromatography on silica gel with DCM. The pure product was obtained as a white solid (0.65 mg, 3.25 mmol, 79 %).

^{1}H NMR (300 MHz, $CDCl_3$): δ = 8.17 (s, 2H), 2.77 (s, 8H).

^{13}C NMR (75 MHz, $CDCl_3$): δ = 198.25, 153.94, 147.00, 125.05, 25.76.

6. Tert-butyl 4-(2,6-diacetylpyridin-4-yl)benzoate (4)

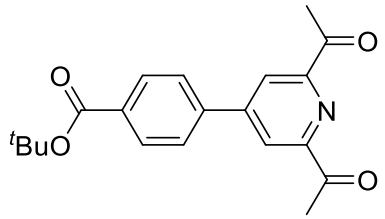

Under argon 4-chloro-2,6-diacetylpyridine (323 mg, 1.63 mmol, 1 eq.), (4-(tert-butoxycarbonyl) phenyl)boronic acid (362 mg, 1.96 mmol, 1.2 eq.), Pd_2dba_3 (52 mg, 0.081 mmol, 0.05 eq), NaI (581 mg, 3.87 mmol, 2.4 eq.) and $HP(tBu)_3BF_4$ (52 mg, 0.163 mmol, 1 eq.) were added to dry DME (15 mL). Then, K_3PO_4 (4.2 mL, 1 M, 2.6 eq.) was added and the reaction mixture was stirred over night at 90 °C. Afterwards, the reaction mixture was poured in 200 mL H_2O and the mixture was extracted with chloroform (3 x 150 mL), washed with brine solution (150 mL), dried over $MgSO_4$, filtered and then the solvent was evaporated under reduced pressure. The crude product was purified by column chromatography using chloroform as eluent. The pure product was obtained as a white solid (439 mg, 1.18 mmol, 80 %).

^{1}H NMR (300 MHz, $CDCl_3$): δ = 8.47 (s, 2H), 8.12 (d, *J* = 8.5 Hz, 2H), 7.78 (d, *J* = 8.4 Hz, 2H), 2.84 (s, 6H), 1.62 (s, 9H).

^{13}C NMR (75 MHz, $CDCl_3$): δ = 199.40, 165.08, 153.62, 149.70, 140.53, 133.35, 130.45, 127.09, 122.47, 81.66, 28.28, 25.79.

7. $[Co^{III}(N_4^{COOtBu})Cl_2]Cl$ (5)

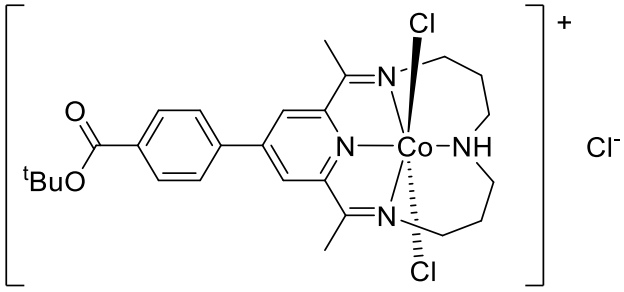

Tert-butyl 4-(2,6-diacetylpyridin-4-yl)benzoate (270 mg, 0.79 mmol, 1 eq.) was dissolved in a mixture of methanol and DCM (1.5 mL : 1.5 mL). A solution of $CoCl_2 \cdot 6\ H_2O$ (188 mg, 0.79 mmol, 1 eq.) in methanol (1 mL) and 3,3'-diaminodipropylamine (0.122 mL, 0.79 mmol, 1 eq.) were then successively

added. Then, glacial acetic acid (0.1 mL) was added to the reaction mixture. The reaction mixture was irradiated under standard microwave conditions for 1 hour at 100 °C. 50 µL of concentrated aqueous HCl (37%) solution in methanol (1 mL) was added and the resulting reaction mixture was degassed for 1 hour with air. The solution was then concentrated under reduced pressure, EtOAc was added causing formation of a precipitate. The precipitate was filtered and dissolved in acetonitrile. Finally, the solvent was removed under reduced pressure to obtain the product as a green solid (436 mg, 0.15 mmol, 90 %).

^{1}H NMR (300 MHz, $CDCl_3$): δ = 8.66 (s, 2H), 8.25 (d, 2H), 8.14 (d, 2H), 5.97 (s, 1H), 4.21 (m, 2H), 3.66 (m, 2H), 3.48 (m, 2H), 3.15 (m, 2H), 2.95 (s, 6H), 2.31 (m, 2H), 2.15 (m, 2H), 1.65 (s, 9H)

8. $[Co^{III}(N_4{}^{COOH})Cl_2]Cl$ (6)

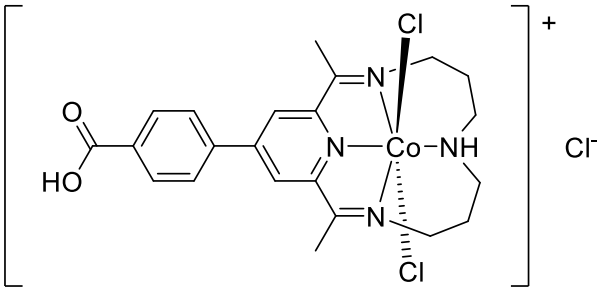

To a solution of $[Co^{III}(N_4{}^{COO\mathit{t}Bu})Cl_2]Cl$ (197.60 mg, 0.329 mmol, 1 eq.) in DCM (8 mL) was added dropwise trifluoroacetic acid (1.09 mL, 16.5 mmol, 50 eq.). The reaction mixture was stirred overnight at room temperature. The solvents were then removed under reduced pressure and the remaining solid was dissolved in acetonitrile. The obtained solution was filtered, and the solvent evaporated under reduced pressure. The product was obtained as a green solid (161 mg, 0.296 mmol, 90 %).

^{1}H NMR (300 MHz, $CDCl_3$): δ = 13.32 (br, 1H), 9.01 (s, 2H), 8.37 (d, 2H), 8.21 (d, *J* = 8.1 Hz, 2H), 6.81 (br t, *J* = 10.6 Hz, 1H), 4.07 (d, *J* = 16.3 Hz, 2H), 3.54 (t, *J* = 14.7 Hz, 2H), 3.18 (q, *J* = 12.1 Hz, 2H), 3.01 (d, *J* = 15.5 Hz, 2H), 2.87 (s, 6H), 2.25 (d, *J* = 15.8 Hz, 2H), 2.09 (d, *J* = 14.2 Hz, 2H).

9. $[Co^{III}(N_4{}^{Bu\text{-}Pyr})Cl_2]Cl$ (**$CoN_4H\text{-}Ph_{Pyr}$**)

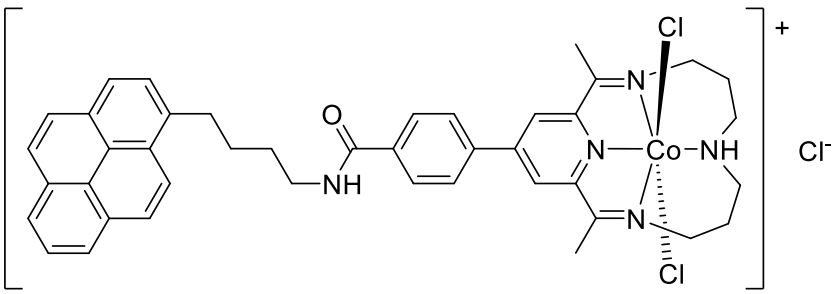

Dry triethylamine (25.7 µL, 0.184 mmol, 1 eq.) (dried over KOH overnight) was added to a solution of $[Co^{III}(N_4^{COOH})Cl_2]Cl$ (100 mg, 0.184 mmol, 1 eq.) in dry DMF (6 mL) under argon. HATU (70,1 mg, 0.184 mmol, 1 eq.) was then added to the reaction mixture at 0 °C. After removing the ice bath the reaction mixture was stirred for 10 minutes at room temperature. A solution of 4-(pyren-1-yl)butyl-1-amine (57.1 mg, 0.184 mmol, 1 eq.) and triethylamine (25.7 µL, 0.184 mmol, 1 eq.) in dry DMF (3 mL) was then added dropwise at 0 °C. The reaction mixture was left stirring overnight at room temperature. Excess diethyl ether (200 mL) was poured into the flask causing a precipitate that was filtered and washed with additional diethyl ether. The residue was dissolved in methanol and 137 µL concentrated HCl (37%) was added and the mixture was stirred for 4 hours at 70 °C. After cooling down to room temperature, the solution was filtered, the filtrate was concentrated to 2 mL under reduced pressure and excess ethyl acetate (200 mL) was added causing a precipitate. The precipitate was dissolved in MeCN, which was then evaporated under reduced pressure to give the pure product (55.5 mg, 0.069 mmol, 38 %) as a green solid.

^{1}H NMR (400 MHz, DMSO-d_6): δ = 9.02 (s, 1H), 8.99 (s, 1H), 8.76 (m, 1H), 8.26 (m, 10H), 8.05 (t, *J* = 7.52 Hz, 1H), 7.99 (d, *J* = 7.60 Hz, 1H), 6.82 (t, *J* = 10.56 Hz, 1H), 4.07 (d, *J* = 15.89 Hz, 2H), 3.54 (t, *J* = 13.54 Hz, 2H), 3.42 (m, 4H), 3.18 (q, *J* = 11.58 Hz, 2H), 3.01 (s, 6H), 2.86 (d, *J* = 10.76 Hz, 2H), 2.26 (d, *J* = 14.76 Hz, 2H), 2.08 (q, *J* = 12.83 Hz, 2H), 1.88 (t, *J* = 7.18 Hz, 2H), 1.76 (t, *J* = 6.52 Hz, 2H).

^{13}C NMR (100 MHz, DMSO-d_6): δ = 178.62, 165.17, 156.82, 151.95, 137.27, 136.92, 136.58, 130.87, 130.38, 129.21, 128.30, 128.03, 127.51, 127.44, 127.16, 126.46, 126.11, 125.70, 124.93, 124.73, 124.22, 124.12, 123.52, 51.10, 49.74, 32.30, 29.11, 28.98, 25.81, 17.51.

IR (ATR): $\tilde{\nu}$ (cm^{-1}) = 3371 (br, N–H).

UV/vis: λ (nm) = 266 (ε = 6161 L mol^{-1} cm^{-3}), 277 (ε = 8429 L mol^{-1} cm^{-3}), 314 (ε = 3615 L mol^{-1} cm^{-3}), 328 (ε = 4722 L mol^{-1} cm^{-3}), 344 (ε = 4670 L mol^{-1} cm^{-3}), 419 (ε = 601 L mol^{-1} cm^{-3}).

MS (ESI+, MeOH): m/z = 762.5 (100% $[Co^{III}(N_4^{Bu\text{-}Pyr})Cl_2]^+$), 726.4 (24% $[Co^{III}(N_4^{Bu\text{-}Pyr})Cl]^{2+}$) , 690.6 (14% $[Co^{III}(N_4^{Bu\text{-}Pyr})]^{3+}$).

10. $[Co^{III}(N_4{}^{Bu})Cl_2]Cl$ (**CoN_4H-Ph_{Bu}**)

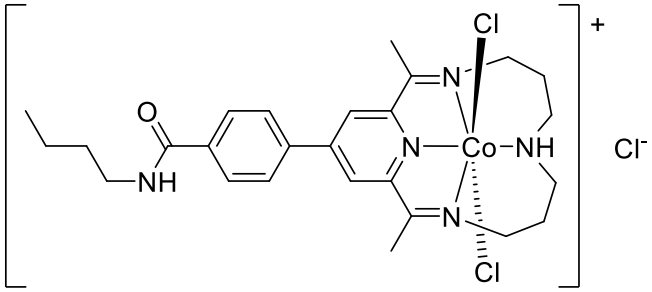

Dry triethylamine (19.2 µL, 0.138 mmol, 1 eq.) (dried over KOH overnight) was added to a solution of $[Co^{III}(N_4{}^{COOH})Cl_2]Cl$ (72.3 mg, 0.138 mmol, 1 eq.) in dry DMF (5 mL) under argon. HATU (52.3 mg, 0.138 mmol, 1 eq.) was then added to the reaction mixture at 0 °C. After removing the ice bath the reaction mixture was stirred for 10 minutes at room temperature. A solution of *n*-butylamine (13.6 µL, 0.138 mmol, 1 eq.) (dried over KOH overnight) and triethylamine (15.3 µL, 0.190 mmol, 1 eq.) in dry DMF (2 mL) was then added dropwise at 0 °C. The reaction mixture was left stirring overnight at room temperature. Excess diethyl ether (150 mL) was poured into the flask causing a precipitate that was filtered and washed with additional diethyl ether. The residue was dissolved in methanol and 99 µL concentrated HCl (37%) was added and the mixture was stirred for 4 hours at 70 °C. After cooling down to room temperature, the solution was filtered, the filtrate was concentrated to 2 mL under reduced pressure and excess ethyl acetate (200 mL) was added causing a precipitate. The precipitate was dissolved in MeCN, which was then evaporated under reduced pressure to give the pure product (26.3 mg, 0.044 mmol, 32 %) as a green solid.

^{1}H NMR (400 MHz, DMSO-d_6): δ = 9.02 (s, 2H), 8.77 (s, 1H), 8.37 (d, *J* = 6.14 Hz, 2H), 8.15 (d, *J* = 7.28 Hz, 2H), 6.81 (m, 1H), 4.06 (m, 2H), 3.52 (m, 2H), 3.16 (m, 2H), 3.01 (s, 6H), 2.87 (m, 2H), 2.25 (m, 2H), 2.07 (m, 2H), 1.58 (m, 4H), 1.37 (m, 2H), 0.93 (t, *J* = 6.99 Hz, 3H).

^{13}C NMR (100 MHz, DMSO-d_6): δ = 178.36, 164.86, 156.57, 151.69, 136.98, 136.33, 129.85, 129.55, 128.46, 128.12, 127.86, 125.60, 50.94, 49.55, 30.99, 27.57, 25.66, 19.46, 17.47, 13.53.

CoN_4H-Ph_{Pyr}|MWCNTs electrode preparation

A 3 mg mL^{-1} MWCNT (NC7000, Nanocyl) dispersion in EtOH was prepared by sonication for 30 min in an ultrasonic bath. 30 µL of this dispersion was deposited at the surface of a glassy carbon electrode (1.6 mm diameter, from ALS) and let to dry in air for 15 min in order to generate relatively homogeneous deposit (0.28 cm^2 of geometrical area). The MWCNT electrode was then modified by soaking the film in a solution (40 µL) of **CoN_4H-Ph_{Pyr}** at a controlled concentration (from 0.5 to 20 mM)

in DMF for 6 min. The modified **CoN_4H-Ph_{Pyr}**|MWCNT electrode was then washed with DMF in order to remove the excess unbound **CoN_4H-Ph_{Pyr}** and then with water to wash off the DMF.

Electrochemistry

Electrochemistry experiments were carried out with Biologic SP-300 and VSP-300 potentiostats. Electrochemistry in organic media was carried out in MeCN under argon or CO_2 atmosphere with a 3-electrode setup using a glassy carbon (GC) as working electrode (1.6 mm diameter, from ALS), a homemade Ag/AgCl (KCl sat., prepared by anodization of a Ag wire in a 1M KCl solution and subsequent storage in KCl saturated solution in a glass tube with a Vycor frit separator) as reference electrode and a Pt wire as counter electrode. Controlled potential electrolysis (CPE) were performed using a 2-compartment cell separating the counter (Pt wire) from the reference (homemade Ag/AgCl, KCl sat.) and the working electrode (GC disk, 13 mm diameter, ALS). Ferrocene was added at the end of each experiment to serve as an internal reference. Aqueous electrochemistry (CV and CA) was performed in $KHCO_3$ 0.5 M under argon or CO_2 saturated atmosphere and electrolyte in a homemade 2-compartment cell separated by a frit (porosity 4). The MWCNT modified GC electrode (1.6 mm diameter, from ALS, 6 mm diameter once modified to give an active geometrical area of 0.28 cm^2) was used as working electrode, a homemade Ag/AgCl (KCl sat.) as reference electrode and a Pt wire as counter electrode. All experiments were performed at room temperature. First scan direction was always cathodic, starting at open circuit potential of the working electrode (e.g. at the Co^{III} state) with no applied pretreatment. For the CV and CA, iR drop was not compensated except for the scan rate dependency study were ZIR method was used and 85% of the measured resistance (R_u) was compensated (R_c). GC electrodes were cleaned and polished with diamond paste (1 µm from Struers) on a 1-µm grain polishing mat (MD-Nap, from Struers) in between every experiment using a polishing machine (Struers, LaboPol-1). CPE and CA were performed under constant stirring with a 15 mm stirring bar and at approximately 1000 rpm.

XPS

Samples for XPS were prepared by depositing 150 µL of a 3 mg mL^{-1} MWCNT (NC7000, Nanocyl) dispersion in EtOH at the surface of a glassy carbon electrode (13 mm diameter, from ALS). The deposit was then let to dry in air for 15 min in order to generate relatively homogeneous deposit. The MWCNT electrode was then modified by soaking the film in a solution (200 µL) of **CoN_4H-Ph_{Pyr}** (15 mM) in DMF for 6 min. The modified **CoN_4H-Ph_{Pyr}**|MWCNT electrode was then washed with DMF in order to remove the excess unbound **CoN_4H-Ph_{Pyr}** and then with water to wash off the DMF. The core-level peaks were

recorded with a constant pass energy of 23.3 eV. The XPS spectra were fitted with CasaXPS 2.3 software using the Shirley background. Binding energies are referenced with respect to adventitious carbon (C 1s BE = 284.8 eV).

Operando XAS spectroscopy measurements

Cobalt K-edge X-ray Absorption Spectroscopy (XAS) analysis was performed at the CRG-FAME beamline (BM30) of the European Synchrotron Radiation Facility (ESRF, Grenoble, France). The ring is operated at 6 GeV with a nominal current of 200 mA in 7/8+1 mode. The beamline is equipped with a liquid-nitrogen-cooled double crystal Si(220) monochromator surrounded by two Rh-coated mirrors for harmonic rejection.[3] The beam size on the sample is 200x100 μm^2 (HxV, FWHM). The monochromator was energy calibrated by measuring the Co K-edge absorption spectrum of a metallic Co foil and setting the first maximum of its 1st derivative at 7709 eV. The Co K-edge energy region was scanned in the 7400-8700 eV range.[4] The X-ray absorption spectra of the solutions were recorded in the fluorescence mode with a 13-elements Ge solid-state detector (Canberra). Three to nine scans were acquired over different spots of the samples to avoid radiation damage, and merged in the final spectrum. Reference compounds were prepared as pellets diluted in boron nitride and measured in the transmission mode. The spectrum of the Co_3O_4 oxide measured on the same beamline was downloaded from the SSHADE database [DOI: 10.26302/SSHADE/EXPERIMENT_IM_20120926_001],[5] the details of its acquisition have been reported previously.[6]

XAS data reduction and normalization were performed with standard methods using the Athena software implemented in the Demeter suite.[7] Scattering amplitudes and phase shifts for *ab initio* EXAFS fitting were calculated with the code FEFF8, implemented in the Artemis software.[7,8] The initial structure for the *ab initio* calculations was downloaded from the Cambridge Structural Database (ID: DAWDAK).[9]

The amplitude reduction factor S_0^2 was estimated as 0.8 over the reference compounds. The fits to the experimental data were performed with the Artemis program, using a Levenberg-Marquardt non-linear least-squares minimization algorithm. The spectra were Fourier Transformed in the k range 2.3-12 $Å^{-1}$, then fitted in the real space, in the range [1.0-2.2] Å.

Modified electrode samples **CoN_4H-Ph_{Pyr}**|MWCNT for operando measurements were prepared by first depositing 90 µL of a 3 mg mL^{-1} of MWCNT in EtOH on a 1 cm^2 disk at the surface of a 75-µm-thick flexible graphite foil (Goodfellow, C-00-FL-000105). After letting the deposit dry for 15 minutes, 120 µL of a 7.5 mM solution of **CoN_4H-Ph_{Pyr}** was deposited at the surface of the MWCNT and let to soak for

10 minutes. The deposit was then washed successively with DMF and milli-Q water and let dry for another 10 min. Then, nail polish was layered onto the graphite foil around the MWCNT layer, to prevent the bare graphite foil area to be electrochemically active. The modified graphite foil was then mounted as the working electrode in a photoelectrochemical cell (PECC-2 from Zahner) in a 3-electrode setup with a homemade Ag/AgCl electrode as reference electrode and a Pt wire as counter electrode. The cell was filled with aqueous $KHCO_3$ at 0.5M and degassed either with N_2 or CO_2 using a peristatic pump (VWR PP1300) to flow the degassed electrolyte in and and out the cell.

EXAFS data treatment and analysis

The XANES spectra of the Co-catalyst as-prepared, or at the electrode in aqueous electrolyte solution before and after CA are reported in Figure S10A, along with the spectra of the reference compounds. The Co catalyst as-prepared shows the features reported for a tetradentate macrocyclic Co complex $[LCo^{III}Cl_2]^+$ bearing two chlorides as axial ligands: a weak pre-peak at ~ 7709 eV, and a pronounced shoulder on the rising edge at ~7722 eV.[10,11] The low-intensity and featureless pre-peak corresponds to Co in octahedral coordination[11]: in 3d transition metals, this spectral feature is due to 1s→3d transitions and its intensity increases with the degree of 3d-4p mixing, i.e. the more the metal site deviates from a centrosymmetric coordination environment.[12] Therefore, a weak pre-peak is indicative of a centrosymmetric octahedral binding site. The shoulder at ~7722 eV is a fingerprint for the presence of axial Cl^-, as expected in this Co-catalyst. [10,11]

With respect to the spectrum of the as-prepared catalyst, the spectra of the catalyst in solution before and after CA (showing nearly identical spectral features between them), highlight a sharper rising edge, with no feature on it. Both spectra show a weak pre-peak with no major changes in comparison with the as-prepared powder. These spectral modifications at the white line position have been observed before as a consequence of the substitution of the Cl^- with two axial aqua ligands, both in experimental and in DFT-calculated XANES spectra.[10] It is worth to mention that the loss of one or two axial ligands would induce the appearance of a feature at ~7115 eV due to 1s→4p transitions, as the one that we can observe in the CoPc reference compound (Fig. S10A), and as previously reported for similar Co-macrocyclic compounds.[13,14] Finally, a direct comparison between the spectra of **CoN_4H-Ph_{Pyr}** and the spectra of the Co_3O_4 oxide and of metallic Co highlights that no such species are detected in the probed area of the electrode.

Therefore, from the fingerprint XANES analysis we deduce that, upon immersion of the **CoN_4H-Ph_{Pyr}** modified electrode in the aqueous electrolyte, the axial Cl^- ligands of the octahedral Co center are substituted, most probably by two water molecules. After CA, the Co coordination sphere is unchanged

and its 3+ oxidation state is restored, as proven by the comparison between the derivative XANES spectra before and after CA (Fig. S10A, inset) that show identical features and no overt energy shift. Indeed, a reduction of the Co^{III} center to Co^{II} would cause the X-ray absorption edge to shift of ~2.3 eV towards lower energy.[15,16]

A further proof of the replacement of two axial Cl^- with aqua ligands in solution can be obtained by the quantitative analysis of the EXAFS region of the spectra: the FT EXAFS spectrum of the solid Co-complex (Fig. S10B) shows two well resolved first-shell contributions. When these data are fitted *ab initio* using as the starting model the structure of a cobalt(III) macrocyclic Schiff-base complex $[Co^{III}(CR)Cl_2]ClO_4$,[17] we obtain an excellent agreement with the experimental data, that confirms the presence of four N/O atoms at 1.96±0.03 Å and two Cl atoms at 2.24 ±0.02 Å (Table S1, Fig. S10B). In contracts, the FT-EXAFS spectra of **CoN_4H-Ph_{Pyr}** in solution (Fig. S10B) show no contribution in the spectral region assigned to Cl, and an increase of ~50% in the intensity of the peak assigned to N/O. This further supports the substitution of two Cl^- with aqua ligands at the electrode in solution.

Co-neighbors	R [Å]	σ^2 [Å^2]	ΔE_0 [eV]	R_{fit} [%]
2 Cl	2.24 (2)	0.003 (1)	0 (2)	1.0
4 N/O	1.96 (3)	0.009 (2)		

Table S1: Structural (R, interatomic distances) and dynamical (σ^2, Debye-Waller factors) parameters obtained by ab initio fitting of the experimental EXAFS spectrum of the as-prepared Co-catalyst. ΔE_0 is a standard parameter corresponding to a shift in the energy origin common to all scattering contributions. R_{fit} is the goodness-of-fit, calculated as $\Sigma(\chi_{exp}-\chi_{fit})^2/\Sigma(\chi_{exp})^2$, where χ_{exp} is the experimental data point, and χ_{fit} the corresponding point in the best-fitting curve.

Inductively coupled plasma atomic emission spectroscopy (ICP-AES)

Samples for ICP-AES were prepared by dispersing the (catalyst)/MWCNT deposits off the GC surface in 0.5 mL of a concentrated (65%, ultrapure from Chemlab) HNO_3 solution. The dispersion was sonicated for 1h and let to sit overnight. 100 µL of concentrated sample solutions were then added to 6 mL of a 10% HNO_3 solution. Before analyzing the samples, the solutions were filtered over a regenerated cellulose disposable syringe filter (pore size: 0.2 µm) to remove the dispersed MWCNT aggregates.

Electrolyte samples were prepared with 65%, ultrapure from Chemlab HNO_3 solution. As the cobalt content of the samples was fairly low, we used a dosed addition technique to increase the Co concentration above the detection threshold and improve sensitivity and signal-to-noise ratio of our ICP. 2.5 mL of sample is treated with 1.5mL of nitric acid containing 130 µg/L of Co so at least a minimal concentration of 50 µg/L. Samples were diluted in 10% nitric acid to a final volume of 6 mL prior to analysis by inductively coupled plasma atomic emission spectroscopy (ICP-AES) on an Agilent ICP 725 used in radial reading mode. A standard range of Co in 10% nitric acid, (from 3.9 µg/L to 2 mg/L) was prepared for quantification. The calibration curve was performed at the 258.033 nm wavelength specific to Co. The standard deviation is less than 5% for a detection limit of 10 µg/L.

Calculation of $K_{CoN4H\text{-}PhPyr}$ using a fitted Langmuir isotherm

The association constant between **$CoN_4H\text{-}Ph_{Pyr}$** and the MWCNT electrode (K_{Co}, in L M^{-1}) was obtained using the simple Langmuir isotherm:

$$\Gamma_{Co} = \frac{\Gamma_{Co.\ max} \times K_{Co} \times [Co]}{1 + K_{Co} \times [Co]}$$

Where Γ_{Co} is the surface loading (nmol cm^{-2}), $\Gamma_{Co.\ max}$ is the maximum surface loading to reach a monolayer coverage (nmol cm^{-2}) and [Co] is the concentration of **$CoN_4H\text{-}Ph_{Pyr}$** in the soaking solution (M^{-1}).

Laviron analysis

The Laviron analysis for **$CoN_4H\text{-}Ph_{Pyr}$**|MWCNTs was performed using the set of equations below, extracting the slope and intercept values from the trumpet plots in **Erreur ! Source du renvoi introuvable.** and following previous litterature:[18,19]

$$E_{p,c} = E^{0\prime} - \frac{2.3\mathrm{RT}}{\alpha \mathrm{nF}} \log[\frac{\alpha \mathrm{n} \nu \mathrm{F}}{RTk_{app}}]$$

$$E_{p,a} = E^{0\prime} - \frac{2.3\mathrm{RT}}{(1-\alpha)\mathrm{nF}} \log[\frac{(1-\alpha)\mathrm{n} \nu \mathrm{F}}{RTk_{app}}]$$

Where $E_{p,a}$ and $E_{p,c}$ are the potential of the anodic and cathodic peak, respectively, $E^{0'}$ is the formal potential of the observed redox couple (V, obtained by averaging the potential a slow scan rate), R is the ideal gas constant (8.31 J mol^{-1} K^{-1}), T is the temperature (K), α is the electron transfer coefficient, n is the number of electron involved in the process, F is the Faraday constant (96485 C mol^{-1}) , ν is the scan rate (V s^{-1}) and k_{app} is the apparent rate constant (s^{-1}).

Calculation of α and 1– α are obtained from the slopes of the linear fit:

$$Slope_c = \frac{-2.3\mathrm{RT}}{\alpha \mathrm{nF}}$$

$$Slope_a = \frac{-2.3\mathrm{RT}}{(1-\alpha)\mathrm{nF}}$$

ν_c and ν_a can be obtained from the x-intercept as follow:

$$\log \nu_c = \frac{-\mathrm{y} - \mathrm{intercept}}{slope_c}$$

$$\log \nu_a = \frac{-\mathrm{y} - \mathrm{intercept}}{slope_a}$$

Finally, the electron transfer rate k_{app} can then be obtained from α, (1– α), v_c and v_a as follow:

$$k_{app,c} = \frac{\alpha \mathrm{n} \mathrm{F} \nu_c}{\mathrm{RT}}$$

$$k_{app,a} = \frac{\alpha \mathrm{n} \mathrm{F} \nu_a}{\mathrm{RT}}$$

The k_{app} values can then be obtained by averaging the $k_{app,c}$ and $k_{app,a}$. All the k_{ET} for **CoN_4H-Ph_{Pyr}**|MWCNTs at different loadings are plotted in Figure S20.

Product quantification

Gaseous products (CO and H_2) were quantified using a gas chromatograph (Clarus 580, Perkin Elmer) by sampling 50 µL of the headspace in the cathode compartment over the course of the CA measurements. An *8 x 1/8 SS Porapak Q* column and N_2 as carrier gas was used for product separation leading to two analyzer channels. H_2 and O_2 were detected using a thermal conducticity detector (TCD) and gases like CO_2 and CO were detected using a flame ionisation detector (FID).

Potential traces of formate were tentatively quantified using an ion chromatograph (883 Basic IC Plus from MetrOhm). For CPE's in organic solvents, 0.5 mL of post electrolysis electrolyte was dissolved in 4.5 mL deionized water while 0.5 mL of aqueous electrolyte was diluted in 1.5 mL for CAs performed in aqueous media, before being injected into the IC. Milli-Q water was used as eluent.

FE, TONs and TOFs calculations

Faradaic efficiencies were calculated as follow:

$$FE_{\mathrm{prod.}} = \frac{2 \times n_{\mathrm{prod.}} \times \mathrm{F}}{\mathrm{q}} \times 100$$

Where $FE_{prod.}$ is the faradaic efficiency for one product (in %), 2 is the number of electrons involved in the catalytic processes (reduction of CO_2 to CO or H^+ to H_2), $n_{prod.}$ is the amount of product detected in the headspace of the cathode compartment using GC (µmol), F is the Faraday constant (C mol^{-1}) and q is the charge passed at the time of a corresponding measurements (C).

Turnover numbers ($TON_{prod.}$) and turnover frequencies ($TOF_{prod.}$) were calculated as follow:

$$TON_{\mathrm{prod.}} = \frac{n_{\mathrm{prod.}}}{\Gamma_{\mathrm{Co}}}$$

$$TOF_{\mathrm{prod.}} = \frac{TON_{\mathrm{prod.}}}{t}$$

Where $n_{prod.}$ is the amount of product (µmol) detected in the headspace of the cathode compartment using GC and Γ_{Co} (mol cm^{-2}) is the loading in Co catalyst (obtained either from electrochemical or ICP measurements) and *t* (s) if the time at which the value is calculated.

Treatment of Data

Except the homogeneous electrochemistry measurements, all experimental measurements were performed at least in triplicates to allow calculate average values and deviations.

These were calculated as follow:

$$x_0 = \sum_i \frac{x_i}{n} \quad \sigma = \sqrt{\sum_i \frac{(x_i - x_0)^2}{(n-1)}}$$

With n the number of experiments, x_0 the unweighted mean value and x_i the value of the sample.

Supporting table and figures

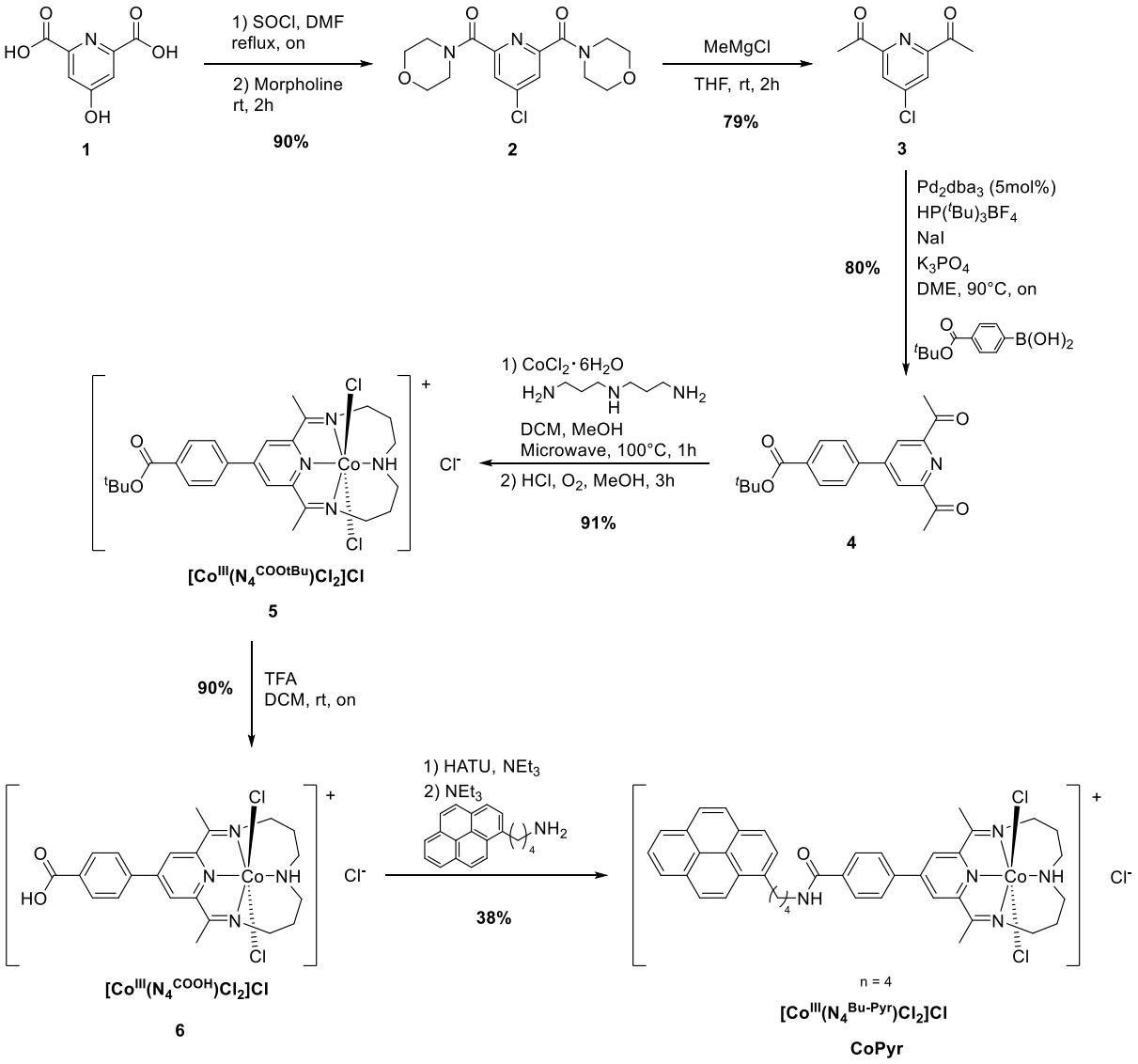

*Figure S1: 6-step synthetic pathway of **CoN4H-Ph$_{Pyr}$**, starting from chelidamic acid.*

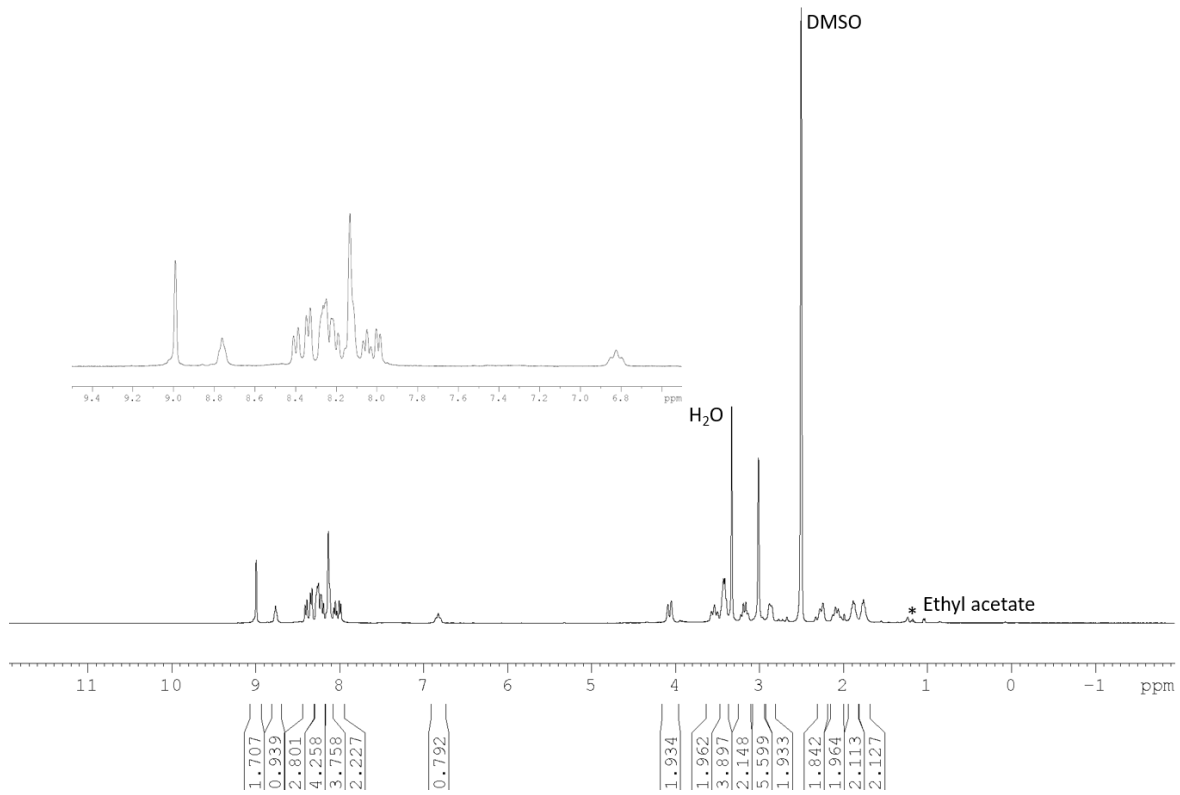

*Figure S2: 1H-NMR Spectra of **CoN4H-PhPyr** in DMSO-d6 at 400 MHz.*

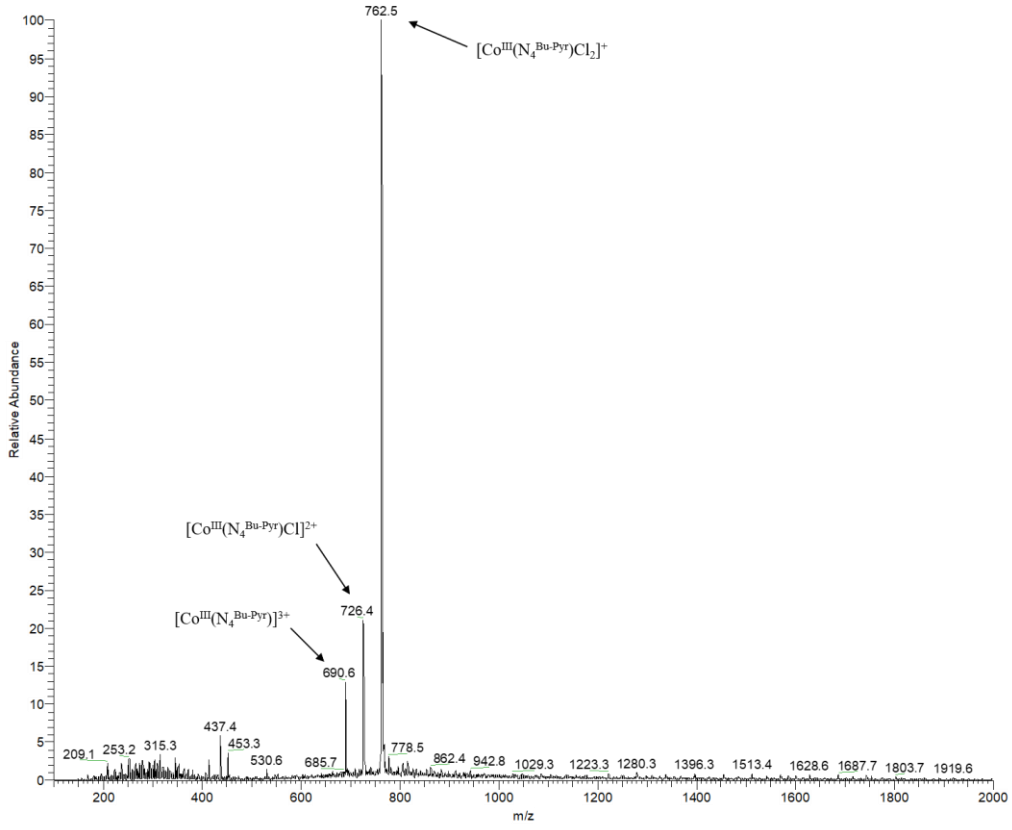

*Figure S3: Positive ESI-MS Spectra of **CoN4H-PhPyr** in MeOH.*

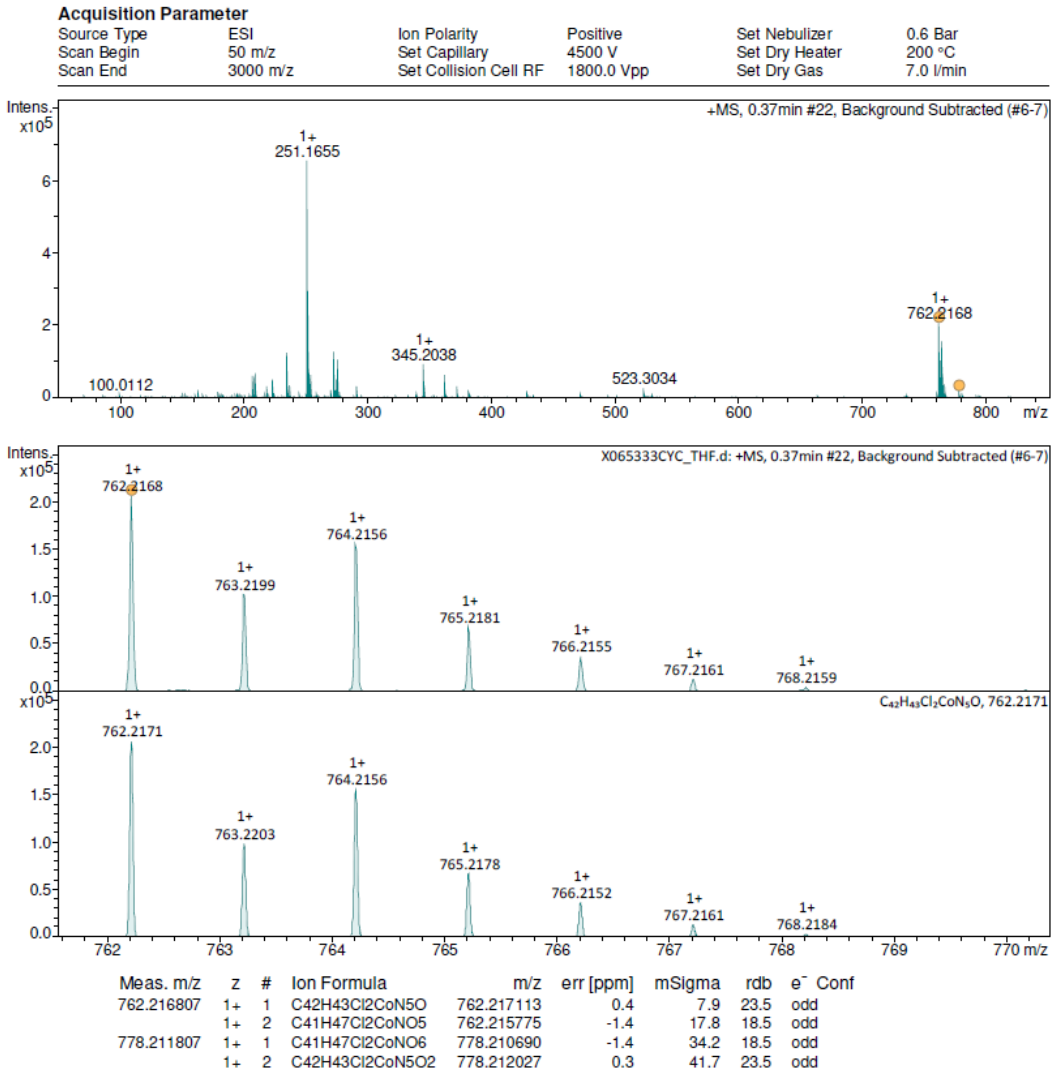

Figure S4: HRMS spectra of ***CoN₄H-Ph$_{Pyr}$*** *in MeOH.*

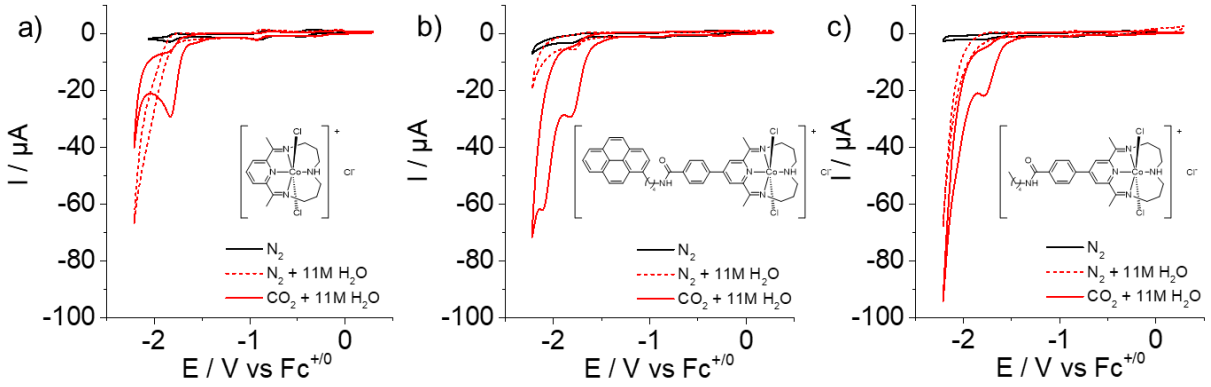

Figure S5: CV of a) ***CoN₄H*** *b)* ***CoN₄H-Ph$_{Pyr}$*** *c)* ***CoN₄H-Ph$_{Bu}$*** *in homogeneous conditions (0.3 mM) in MeCN TBAPF$_6$ 0.1 M under N_2 atmosphere with (red traces) or without (black traces) 11 M of H_2O as proton source and in CO_2 saturated electrolyte with 11 M of H_2O (blue traces). (v = 0.1 V s^{-1}).*

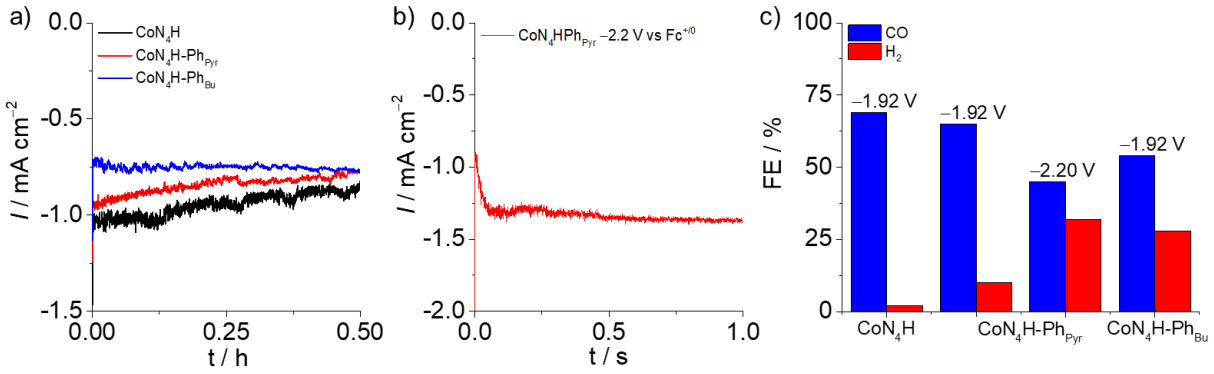

*Figure S6: a) CPE traces of **CoN4H** (black line), **CoN4H-PhPyr** (red line) and **CoN4H-PhBu** (blue line) performed at –1.92 V vs $Fc^{+/0}$; b) CPE of **CoN4H-PhPyr** (red line) at –2.20 V vs $Fc^{+/0}$ with 0.3 mM of catalyst in CO_2-saturated MeCN $TBAPF_6$ 0.1M with 11 M H_2O c) Faradaic efficiency for CO and H_2 obtained after 30 min of CPE with each catalyst tested.*

	$E_{1/2}$ ($Co^{III/II}$)	$E_{1/2}$ ($Co^{II/I}$)	$E_{1/2}$ ($L/L^{\bullet-}$)	$E_{cat/2}$	ic/ip	q / C	FE_{CO} / %	FE_{H2} / %
CoN_4H	–0.41	–0.86	–1.81	–1.75	10.4	–2.30	69	2
CoN_4H-Ph_{Pyr} (CPE @–2.2V)	–0.38	–0.83	–1.74	–1.70	9.2	–2.02 –3.15	65 45	10 32
CoN_4H-Ph_{Bu}	–0.38	–0.83	–1.74	–1.66	10.1	–1.80	54	28

*Table S2: List of the redox couples of each studied compounds (**CoN_4H**, **CoN_4H-Ph_{Pyr}** and **CoN_4H-Ph_{Bu}**) obtained by CV performed in MeCN 0.1M $TBAPF_6$ under argon and passed charge as well as faradaic efficiencies for CO and H_2 measured during CPE at –1.92 V vs $Fc^{+/0}$.*

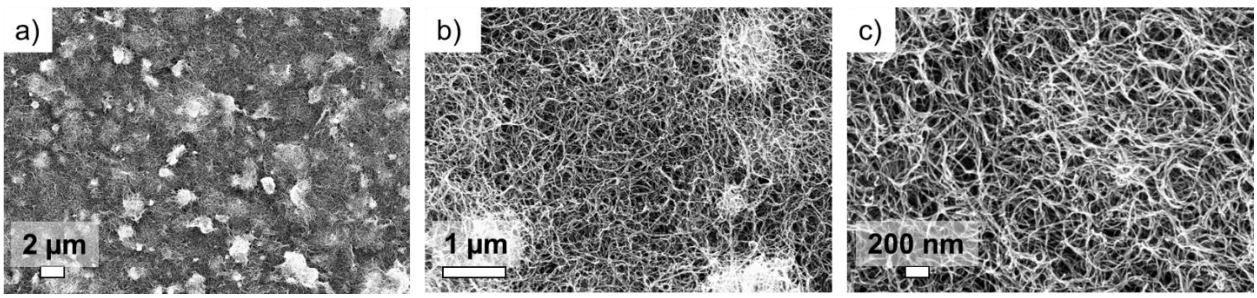

*Figure S7: SEM micrograph of the **CoN_4H-Ph_{Pyr}**|MWCNT films at various magnification.*

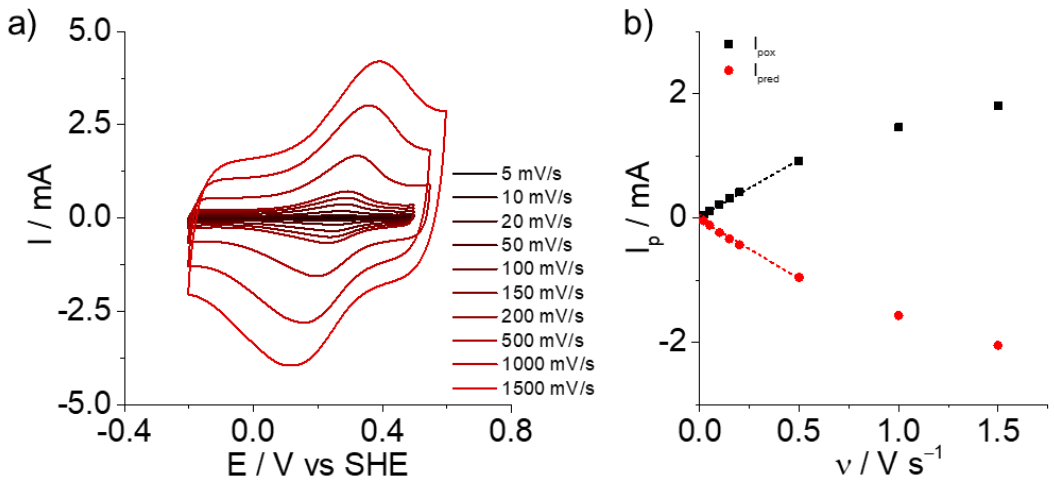

*Figure S8: a) CV at various scan rates of the **CoN_4H-Ph_{Pyr}**|MWCNT modified electrode (5 mM) in $KHCO_3$ 0.5M under N_2 (pH 8.6) b) Evolution of the anodic and cathodic peak current of the $Co^{III/II}$ redox couple of the **CoN_4H-Ph_{Pyr}**|MWCNT modified electrode as function of the scan rate.*

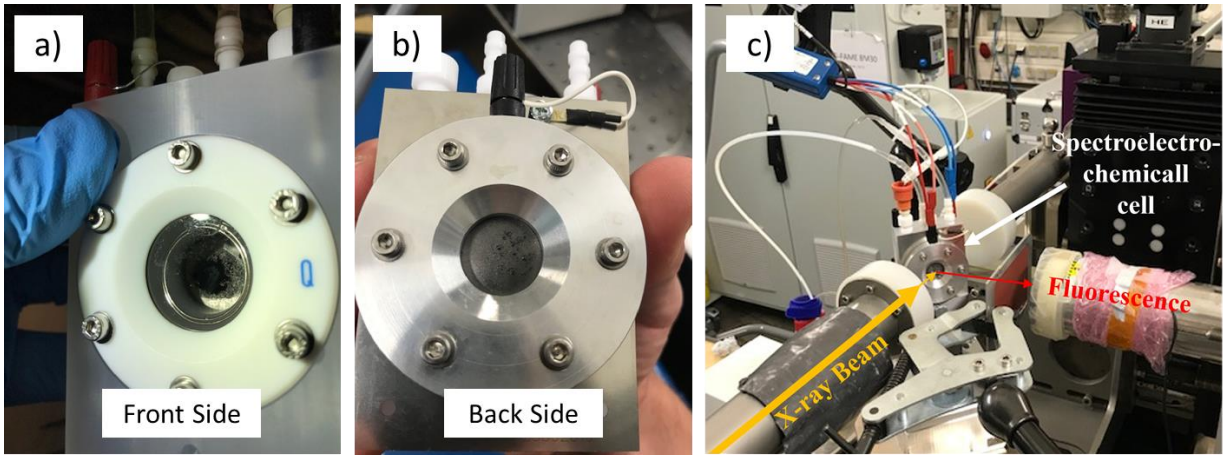

*Figure S9: a) Picture of the front of the PECC-2 cell, showing the **CoN_4H-Ph_{Pyr}**|MWCNT deposit immersed in $KHCO_3$ electrolyte b) picture of the back of the PECC-2 cell showing the graphite foil on which the incident beam is being irradiated c) picture of the general setup showing the cell positioned at 45° between the incoming X-ray beam and the Ge detector to allow fluorescence measurements.*

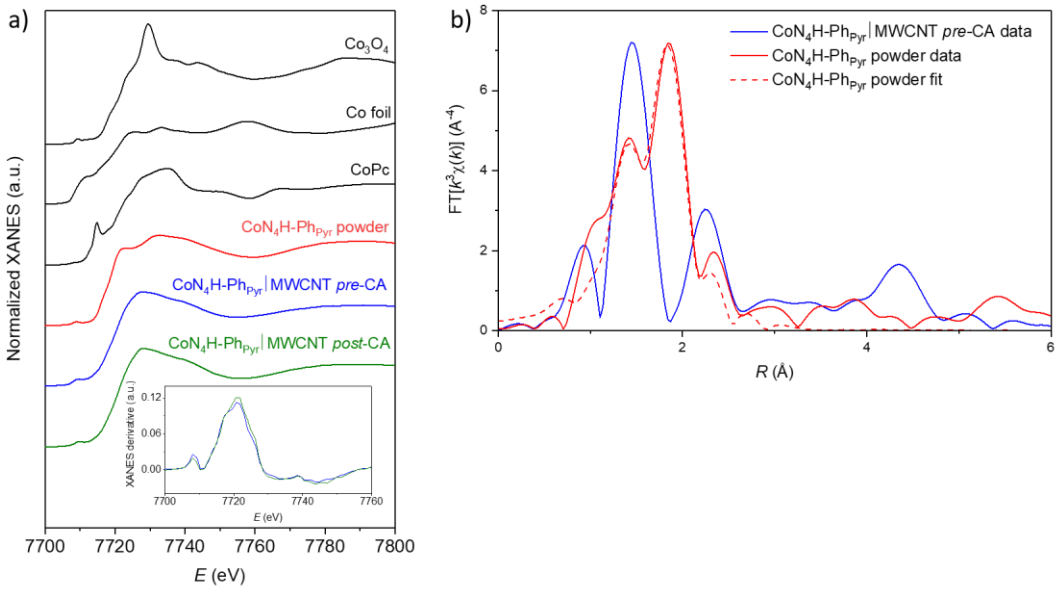

*Figure S10: a) Experimental Co K-edge XANES spectra of the **CoN4H-PhPyr** powder (red line), **CoN4H-PhPyr**|MWCNT pre-CA (blue line) and **CoN4H-PhPyr**|MWCNT post-CA (green) as well as of the reference compounds Co_3O_4, Co foil and CoPc (black lines) b) Experimental (solid curves) and theoretical (dashed) FT-EXAFS spectra of the **CoN4H-PhPyr** powder (red line) and **CoN4H-PhPyr**|MWCNT pre-CA (blue line).*

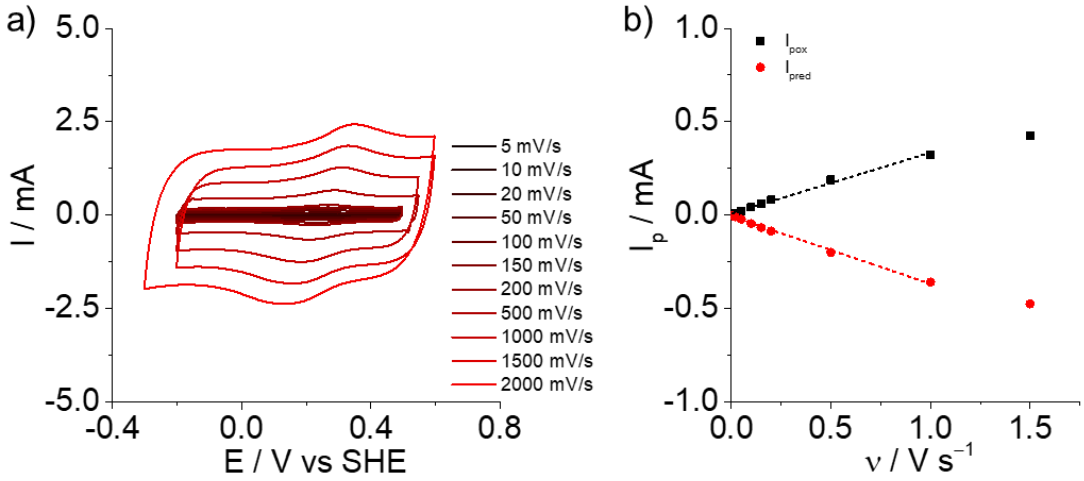

*Figure S11: a) CV at various scan rates of the **CoN4H-PhPyr**|MWCNT modified electrode (0.5 mM) in $KHCO_3$ 0.5 M under N_2 (pH 8.6) b) Evolution of the anodic and cathodic peak current of the $Co^{III/II}$ redox couple of the **CoN4H-PhPyr**|MWCNT modified electrode as function of the scan rate.*

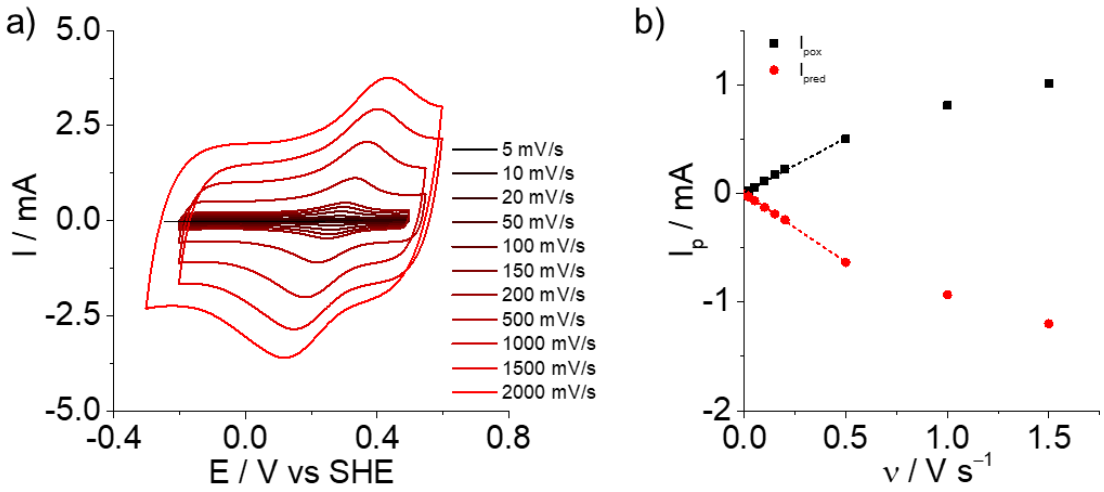

*Figure S12: a) CV at various scan rates of the **CoN4H-PhPyr**|MWCNT modified electrode (1.25 mM) in KHCO3 0.5 M under N2 (pH 8.6) b) Evolution of the anodic and cathodic peak current of the Co$^{III/II}$ redox couple of the **CoN4H-PhPyr**|MWCNT modified electrode as function of the scan rate.*

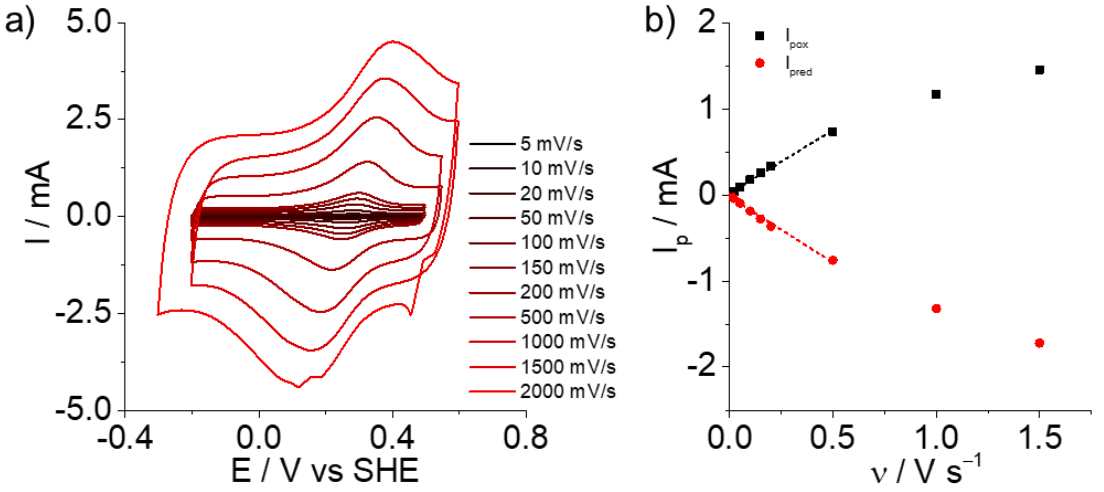

*Figure S13: a) CV at various scan rates of the **CoN4H-PhPyr**|MWCNT modified electrode (2.5 mM) in KHCO3 0.5 M under N2 (pH 8.6) b) Evolution of the anodic and cathodic peak current of the Co$^{III/II}$ redox couple of the **CoN4H-PhPyr**|MWCNT modified electrode as function of the scan rate.*

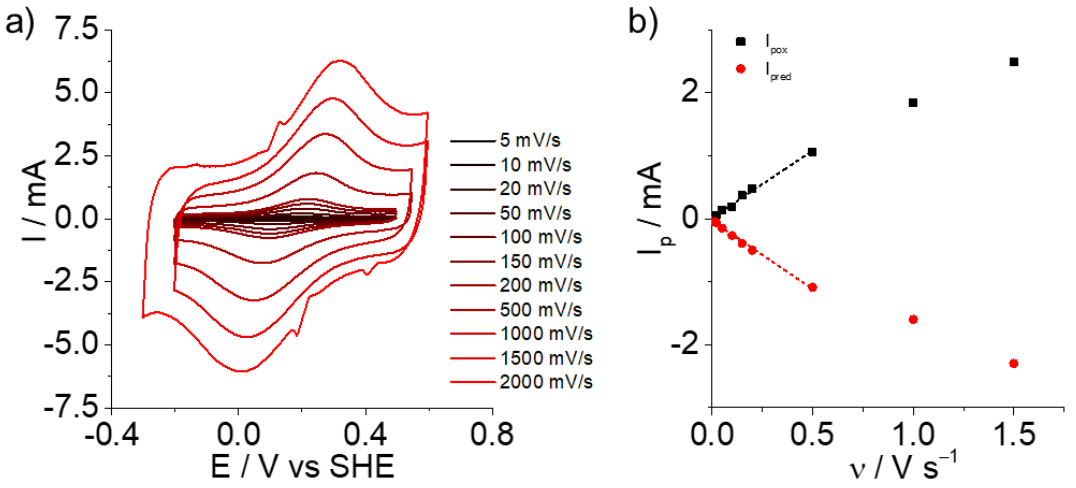

*Figure S14: a) CV at various scan rates of the **CoN₄H-Ph$_{Pyr}$**|MWCNT modified electrode (7.5 mM) in $KHCO_3$ 0.5 M under N_2 (pH 8.6) b) Evolution of the anodic and cathodic peak current of the $Co^{III/II}$ redox couple of the **CoN₄H-Ph$_{Pyr}$**|MWCNT modified electrode as function of the scan rate.*

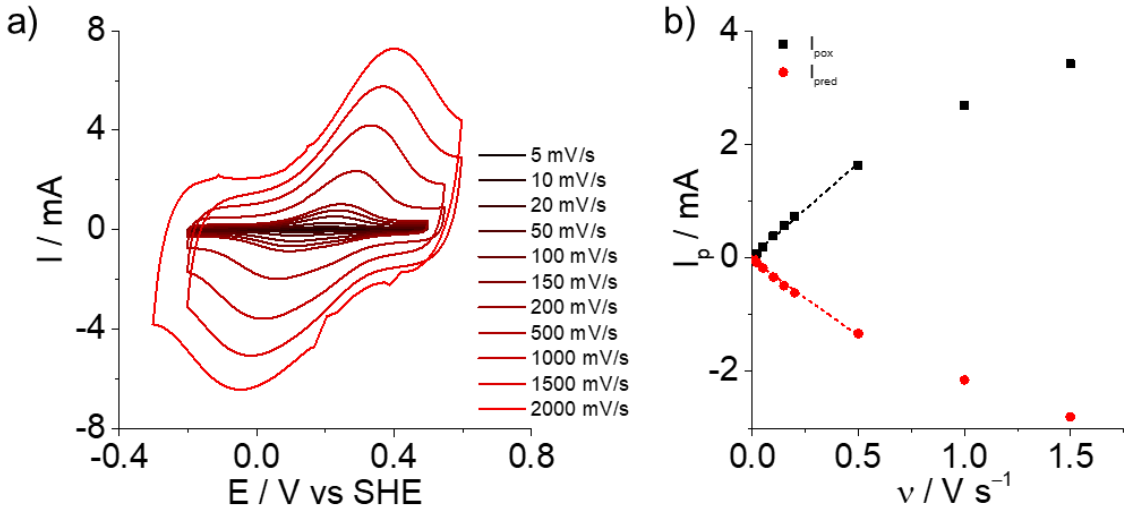

*Figure S15: a) CV at various scan rates of the **CoN₄H-Ph$_{Pyr}$**|MWCNT modified electrode (10 mM) in $KHCO_3$ 0.5 M under N_2 (pH 8.6) b) Evolution of the anodic and cathodic peak current of the $Co^{III/II}$ redox couple of the **CoN₄H-Ph$_{Pyr}$**|MWCNT modified electrode as function of the scan rate.*

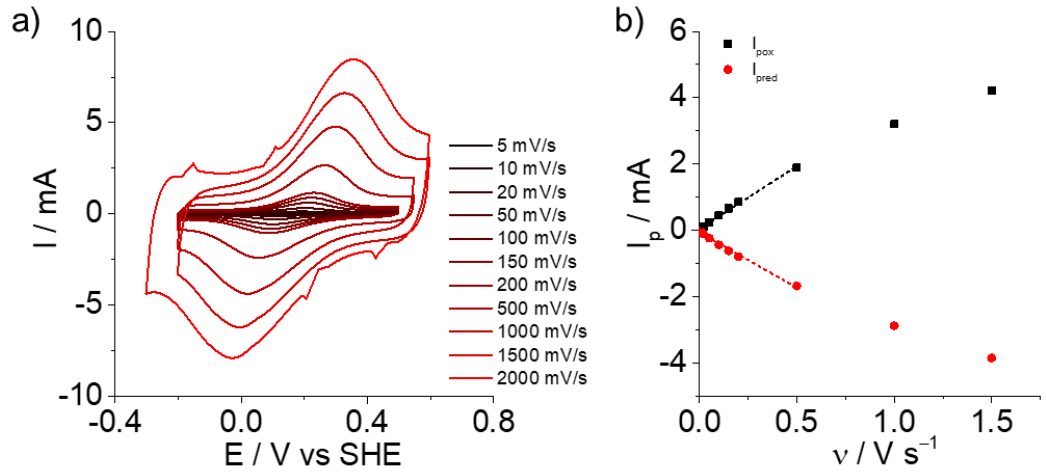

*Figure S16: a) CV at various scan rates of the **CoN₄H-Ph$_{Pyr}$**|MWCNT modified electrode (15 mM) in $KHCO_3$ 0.5 M under N_2 (pH 8.6) b) Evolution of the anodic and cathodic peak current of the $Co^{III/II}$ redox couple of the **CoN₄H-Ph$_{Pyr}$**|MWCNT modified electrode as function of the scan rate.*

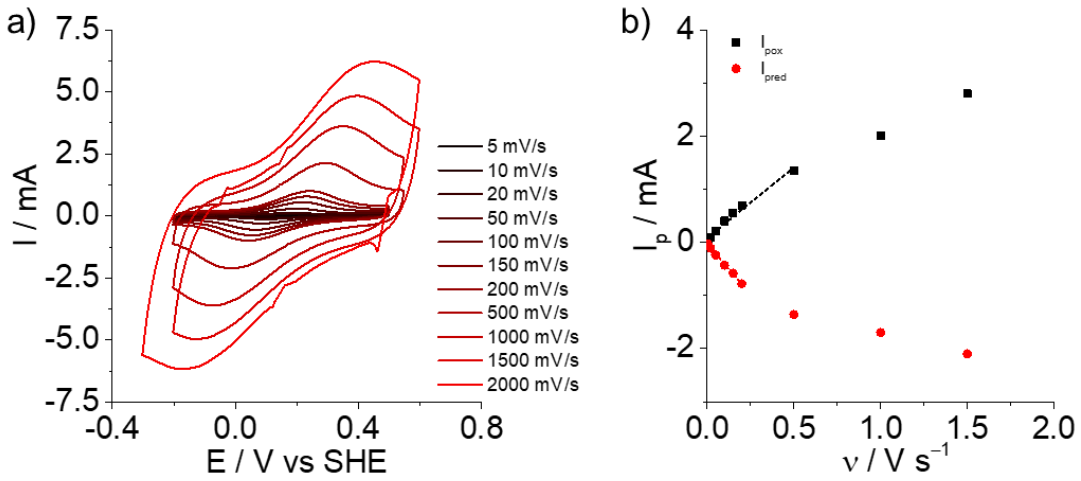

*Figure S17: a) CV at various scan rates of the **CoN₄H-Ph$_{Pyr}$**|MWCNT modified electrode (20 mM) in $KHCO_3$ 0.5 M under N_2 (pH 8.6) b) Evolution of the anodic and cathodic peak current of the $Co^{III/II}$ redox couple of the **CoN₄H-Ph$_{Pyr}$**|MWCNT modified electrode as function of the scan rate.*

Soaking concentration (mM)	**$E_{1/2}$ $Co^{III/II}$ (V vs SHE)**	**$E_{1/2}$ $Co^{II/I}$ (V vs SHE)**	**$\Gamma_{CoN4H\text{-}PhPyr}$ EC (nmol cm^{-2})**	**$\Gamma_{CoN4H\text{-}PhPyr}$ ICP (nmol cm^{-2})**	**$\Gamma_{CoN4H\text{-}PhPyr}$ EC / $\Gamma_{CoN4H\text{-}PhPyr}$ ICP**
0.5	0.26 ± 0.01	-0.45 ± 0.01	3.7 ± 1	/	
1.25	0.27 ± 0.01	-0.43 ± 0.01	8.6 ± 1	13.1 ± 3	66%
2.5	0.27 ± 0.01	-0.41 ± 0.01	13.7 ± 2	/	
5	0.26 ± 0.01	-0.40 ± 0.01	19.8 ± 2	/	
7.5	0.20 ± 0.04	-0.40 ± 0.01	23.3 ± 1	29.6 ± 2	79%
10	0.17 ± 0.01	-0.40 ± 0.01	26.2 ± 6	/	
15	0.15 ± 0.01	-0.39 ± 0.01	38.3 ± 7	37.7 ± 5	101%
20	0.14 ± 0.01	-0.40 ± 0.01	35.5 ± 5	/	

Table S3: Evolution of the redox signals potential observed with the different soaking conditions as well as the surface loadings measured by CV (EC) and ICP-OES (ICP).

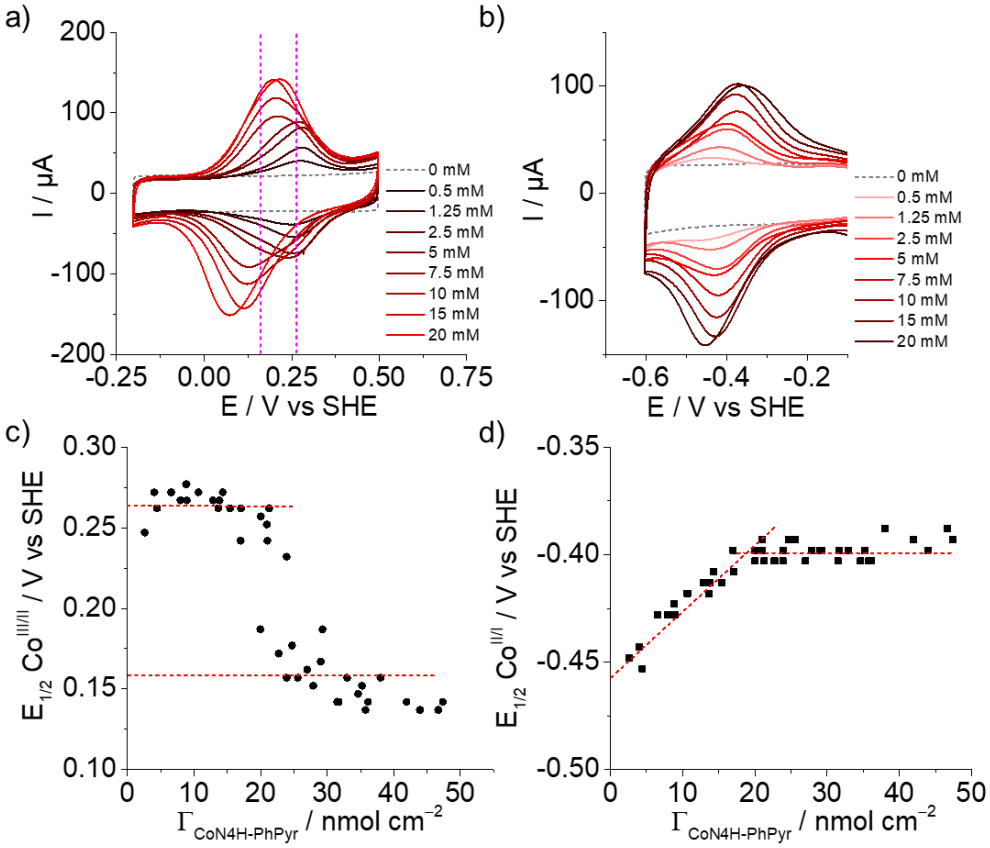

*Figure S18: CV of a) the $Co^{III/II}$ redox couple of the **CoN_4H-Ph_{Pyr}**|MWCNT modified electrode at increasing concentrations and b) the $Co^{II/I}$ redox couple of the **CoN_4H-Ph_{Pyr}**|MWCNT modified electrode at increasing concentrations in $KHCO_3$ 0.5 M under N_2 (pH 8.6) (ν = 0.02 V s^{-1}). Evolution of the $E_{1/2}$ of c) the $Co^{III/II}$ redox couple and the d) the $Co^{II/I}$ redox couple with the surface concentration of **CoN_4H-Ph_{Pyr}**.*

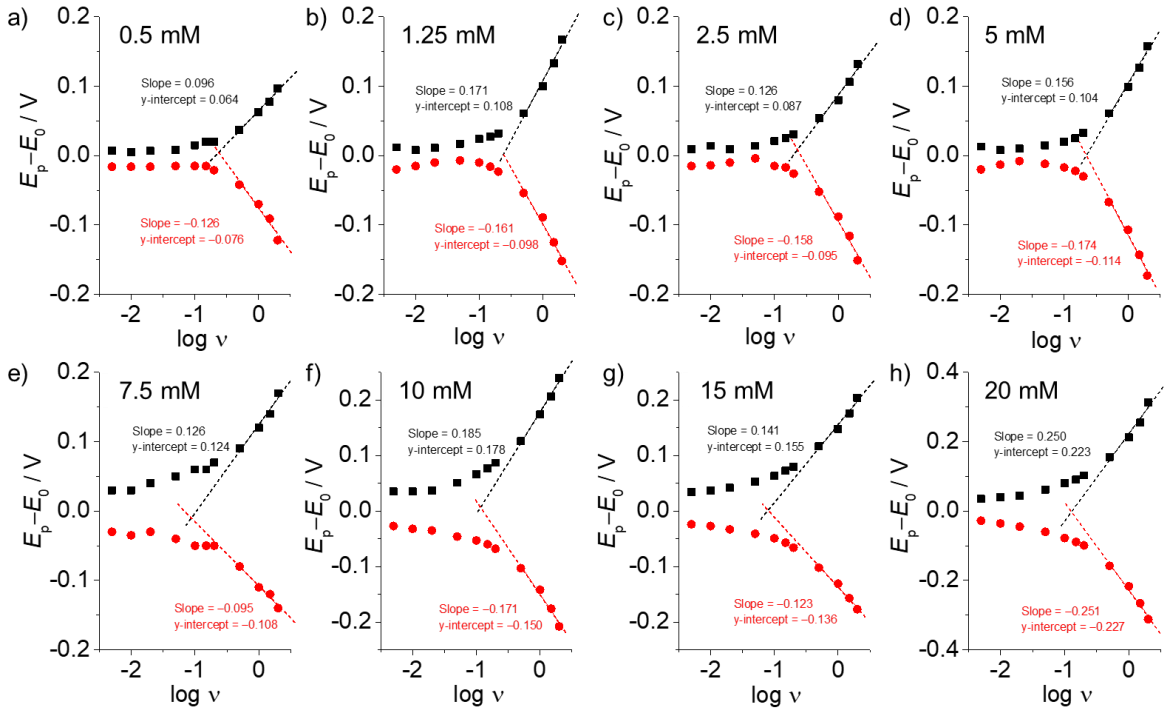

*Figure S19: Laviron plots for **CoN_4H-Ph_{Pyr}**|MWCNT modified with a) 0.5 mM ; b) 1.25 mM ; c) 2.5 mM ; d) 5 mM ; e) 7.5 mM ; f) 10 mM ; g) 15 mM and h) 20 mM obtained from CVs performed in 0.5 M $KHCO_3$ pH 8.5, under argon.*

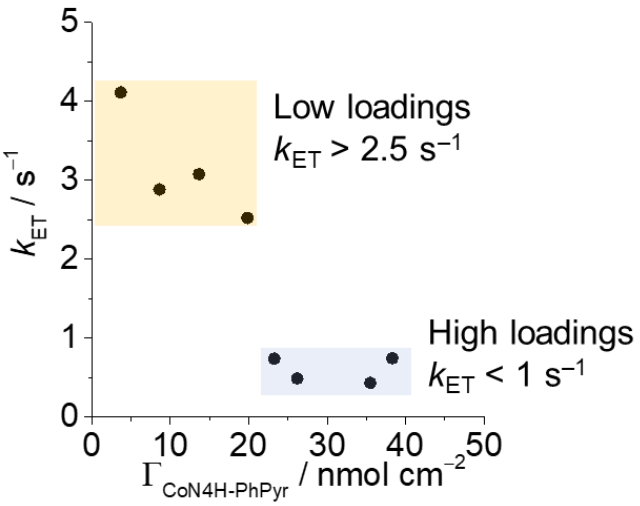

*Figure S20: Electron transfer coefficient obtained from the Laviron plots for **CoN$_4$H-Ph$_{Pyr}$**|MWCNT at increasing surface loadings.*

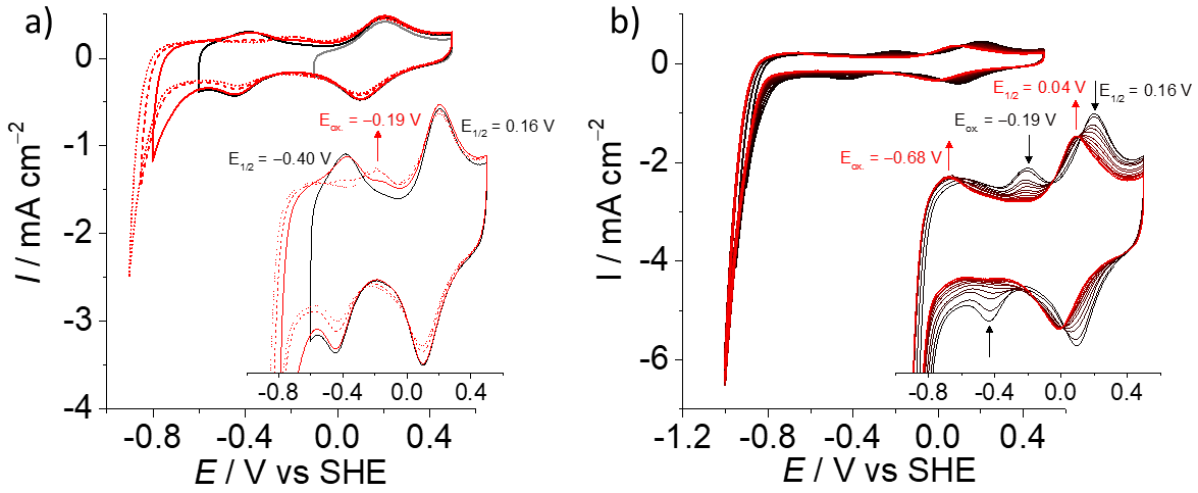

*Figure S21: CV of the Co$^{III/II}$ and Co$^{II/I}$ redox couples of the **CoN$_4$H-Ph$_{Pyr}$**|MWCNT modified electrode modified with 7.5 mM of Co complex in the soaking solution in KHCO$_3$ 0.5 M under N$_2$ (pH 8.6) (v = 0.02 V s^{-1}) a) showcasing the change in reversibility of the Co$^{II/I}$ redox couple (new peak at E$_{ox.}$ = –0.19 V vs SHE); b) showing the formation of the new specie upon applying low potential triggering the catalysis with the concomitant disappearance of the original redox processes over 20 CV cycles (one scan out of two depicted for clarity).*

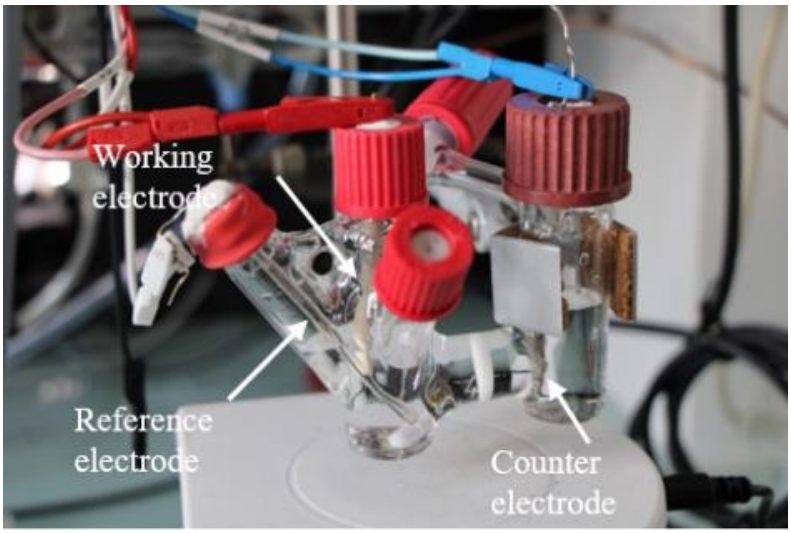

Figure S22: picture of the electrolysis cell used for the aqueous electrochemical characterizations.

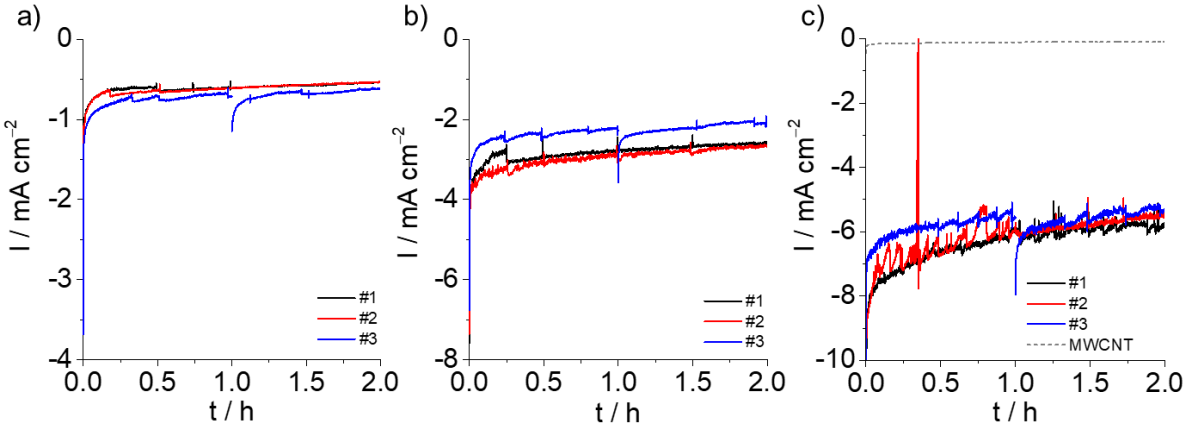

*Figure S23: CA traces triplicates of the **CoN_4H-Ph_{Pyr}**|MWCNT electrode modified with 7.5 mM of Co complex in the soaking solution in CO_2-saturated $KHCO_3$ 0.5 M (pH 7.4) electrolyte at different applied potential a) –0.8 V vs SHE b) –0.9 V vs SHE and c) –1.0 V vs SHE with a blank MWCNT electrode. For all measurements #3 the CA was stopped after 1h to perform CV and characterise the remaining redox response.*

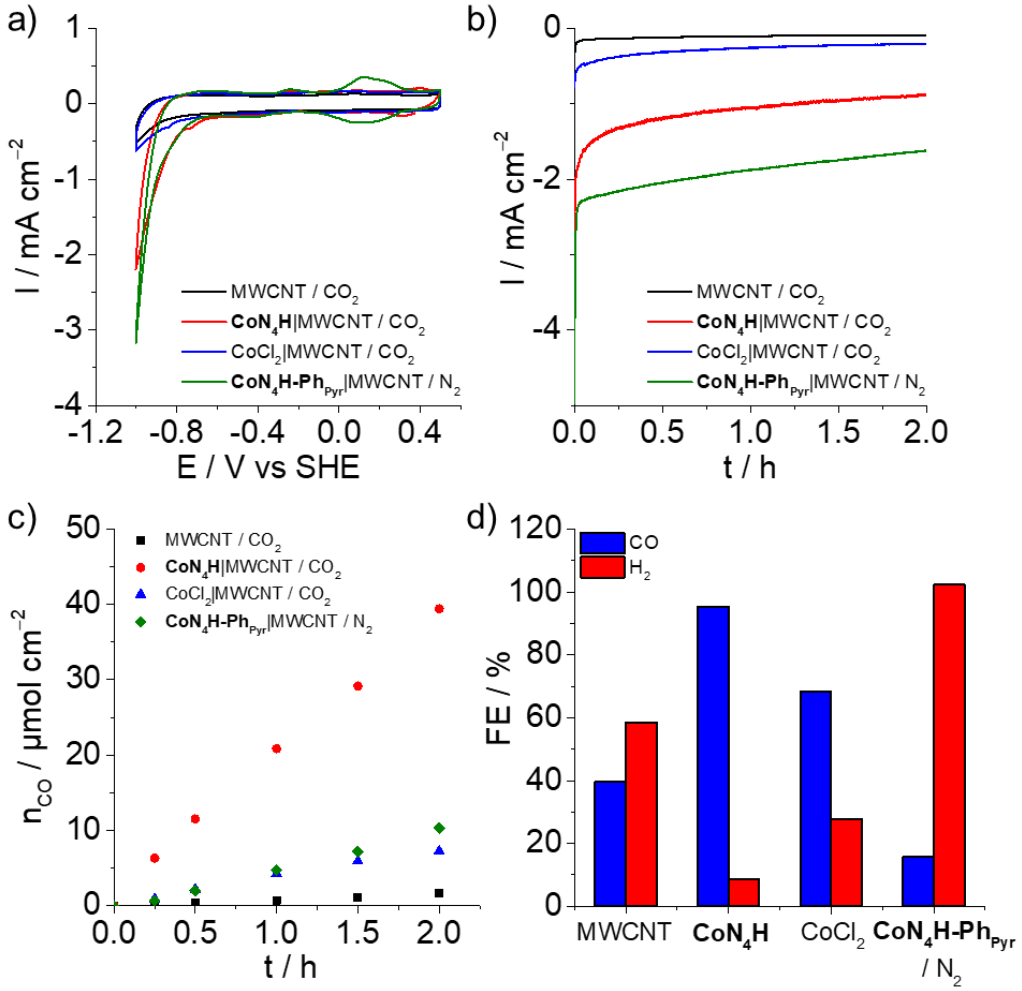

*Figure S24: a) CV traces (v = 0.02 V s^{-1}) b) CA traces c) Amount of CO and d) Faradaic efficiencies for CO (blue columns) and H_2 (red columns) for the control CA experiment performed at –1.0 V vs SHE with bare MWCNTs, **CoN_4H**|MWCNT, MWCNT with 10 µM of $CoCl_2$ in the electrolyte and **CoN_4H-Ph_{Pyr}**|MWCNT. All experiments were performed in 0.5M $KHCO_3$ degassed with CO_2 (pH 7.4) except the control of **CoN_4H-Ph_{Pyr}**|MWCNT under N_2 (pH 8.6).*

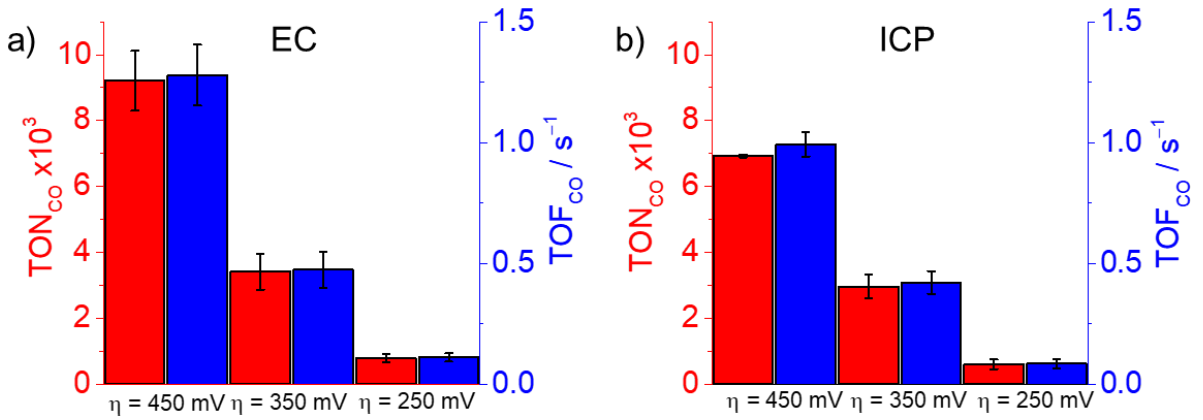

*Figure S25: TON_{CO} and TOF_{CO} of **CoN_4H-Ph_{Pyr}**|MWCNT at various applied overpotential based on a) EC and b) ICP-OES measured catalyst loadings.*

[CoN_4H-Ph_{Pyr}]	$\Gamma_{CoN4H\text{-}PhPyr}$ EC	$\Gamma_{CoN4H\text{-}PhPyr}$ ICP	E_{app}	I_{5min}	I_{2h}	I_{2h} / I_{5min}	n_{CO}	n_{H2}	FE_{CO}	FE_{H2}	TON_{CO} EC	TOF_{CO} EC	TON_{CO} ICP	TOF_{CO} ICP
1.25	8.6 ± 1	13.1 ± 3	–1.0	–6.27 ± 0.5	–4.62 ± 0.4	0.74	183.9 ± 2	9.5 ± 1	94 ± 4	5 ± 1	20110 ± 1607	2.79 ± 0.2	14014 ± 1361	2.04 ± 0.2
7.5	23.3 ± 1	29.6 ± 2	–0.8	–0.78 ± 0.1	–0.56 ± 0.1	0.72	18.1 ± 5	6 ± 1	76 ± 10	25 ± 2	802 ± 126	0.11 ± 0.02	611 ± 152	0.08 ± 0.02
7.5	23.3 ± 1	29.6 ± 2	–0.9	–3.09 ± 0.4	–2.45 ± 0.3	0.79	87.9 ± 11	8.3 ± 2	90 ± 2	8 ± 2	3413 ± 538	0.47 ± 0.1	2968 ± 366	0.42 ± 0.1
7.5	23.3 ± 1	29.6 ± 2	–1.0	–6.88 ± 0.7	–5.54 ± 0.2	0.81	205.3 ± 2	7.8 ± 1	93 ± 3	4 ± 1	9446 ± 1110	1.36 ± 0.2	7096 ± 192	1.02 ± 0.1
15	38.3 ± 7	37.7 ± 5	–1.0	–6.54 ± 0.2	–5.22 ± 0.2	0.80	203.8 ± 7	8.0 ± 1	95 ± 2	4 ± 1	5127 ± 515	0.71 ± 0.1	5408 ± 187	0.79 ± 0.02
0	/	/	–1.0	–0.19	–0.09	0.47	1.7	2.4	40	58	/	/	/	/
CoN_4H		/	–1.0	–1.74	–0.89	0.51	39.4	3.6	95	9	4880	0.87	/	/
$CoCl_2$	/	/	–1.0	–0.54	–0.21	0.39	7.3	2.9	68	28	/	/	/	/
7.5 / N_2	23.3 ± 1	29.6 ± 2	–1.0	–2.36	–1.62	0.69	10.3	63.3	16	102	415	0.06	/	/

Table S4: Table recapitulating EC and ICP surface loadings (Γ, nmol cm^{-2}), current densities (mA cm^{-2}), amount of H_2 and CO product (µmol cm^{-2}), FE (%), TON_{CO} and TOF_{CO} according to EC and ICP loadings for all CA measurements performed at E_{app} = –0.8; –0.9 and –1.0 V vs SHE for 2 h in 0.5 M $KHCO_3$ degassed with CO_2 (pH 7.4). Control experiments are highlighted in orange font.

[CoN_4H-Ph_{Pyr}]	$\Gamma_{CoN4H\text{-}PhPyr}$ EC	$\Gamma_{CoN4H\text{-}PhPyr}$ ICP	E_{app}	$\Gamma_{CoN4H\text{-}PhPyr}$ EC post CA	$\Gamma_{CoN4H\text{-}PhPyr}$ ICP post CA	$\Gamma_{CoN4H\text{-}PhPyr}$ EC post CA / $\Gamma_{CoN4H\text{-}PhPyr}$ EC	$\Gamma_{CoN4H\text{-}PhPyr}$ ICP post CA / $\Gamma_{CoN4H\text{-}PhPyr}$ ICP
1.25	8.6 ± 1	13.1 ± 3	–1.0	6.3 ± 1	6.7	0.73	0.51
7.5	23.3 ± 1	29.6 ± 2	–0.8	15.9 ± 2	14.9 ± 2	0.68	0.50
7.5	23.3 ± 1	29.6 ± 2	–0.9	18.5 ± 4	12.3 ± 2	0.79	0.41
7.5	23.3 ± 1	29.6 ± 2	–1.0	14.5 ± 4	15.5 ± 2	0.62	0.52
15	38.3 ± 7	37.7 ± 5	–1.0	26.2 ± 3	33.3 ± 4	0.68	0.88

Table S5: Table recapitulating EC and ICP surface loadings variation (Γ, nmol cm^{-2}) before and after all CA measurements (2h) performed at E_{app} = –0.8; –0.9 and –1.0 V vs SHE in 0.5 M $KHCO_3$ degassed with CO_2 (pH 7.4).

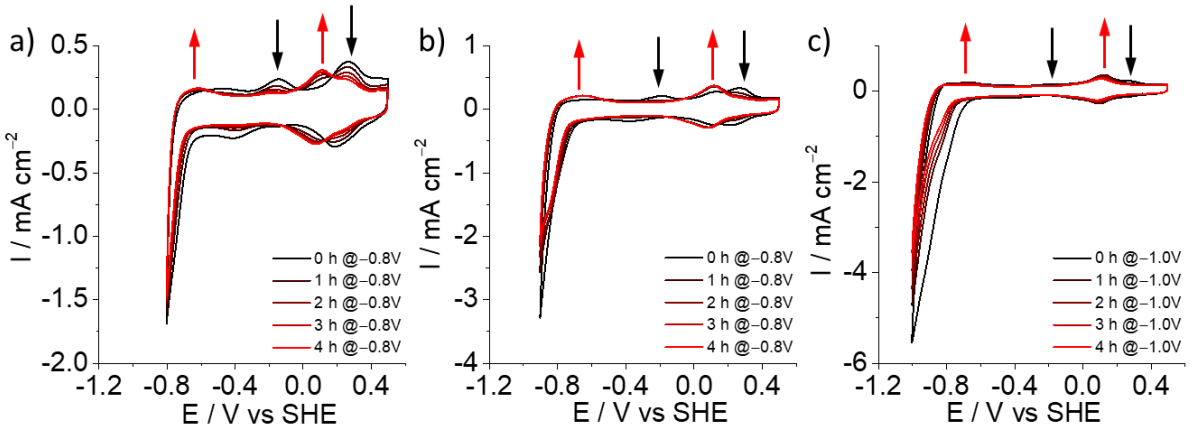

*Figure S26: CV traces of **CoN$_4$H-Ph$_{Pyr}$**|MWCNT electrodes modified with 7.5 mM of Co complex in the soaking solution performed before and after successive 1h CA experiments at a) –0.8 b) –0.9 and c) –1.0 V vs SHE in 0.5 M KHCO$_3$ degassed with CO$_2$ (pH 7.4) (v = 0.02 V s^{-1}).*

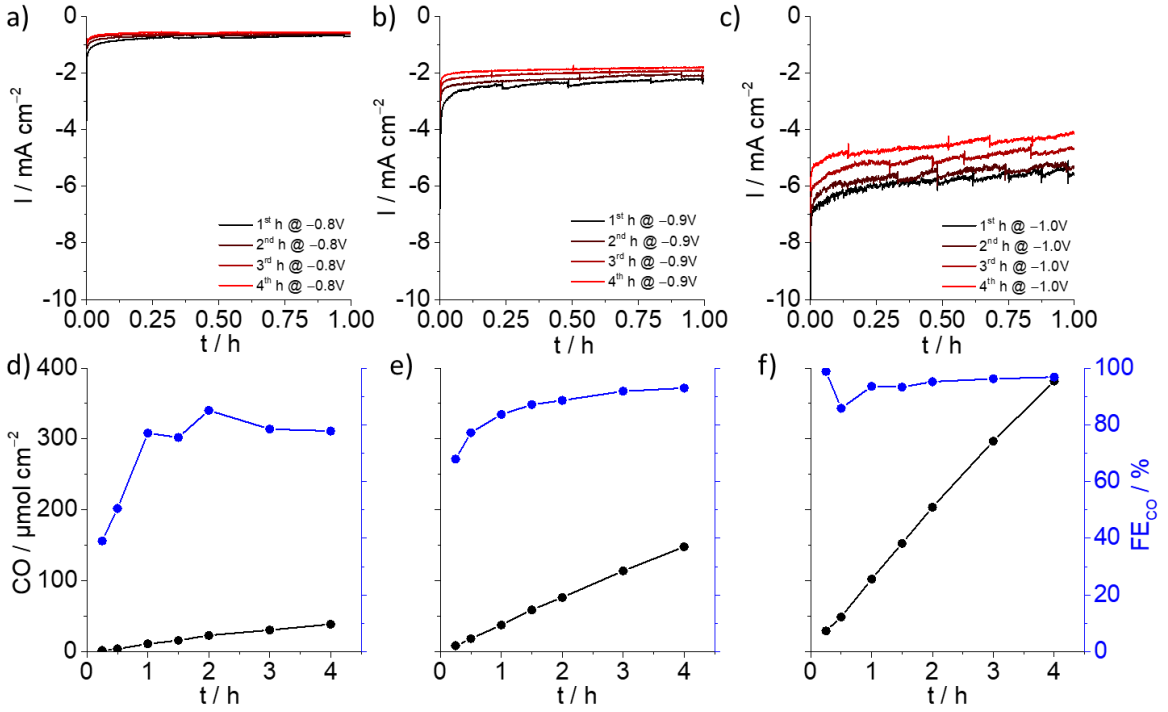

*Figure S27: Traces of four successive 1 h CA experiments of **CoN$_4$H-Ph$_{Pyr}$**|MWCNT electrodes modified with 7.5 mM of Co complex in the soaking solution at a) –0.8 b) –0.9 and c) –1.0 V vs SHE in 0.5 M KHCO$_3$ degassed with CO$_2$ (pH 7.4) and the evolution of the amount of CO produced (black dots and traces) and FE$_{CO}$ (blue dots and traces) overtime at d) –0.8 e) –0.9 and f) –1.0 V vs SHE.*

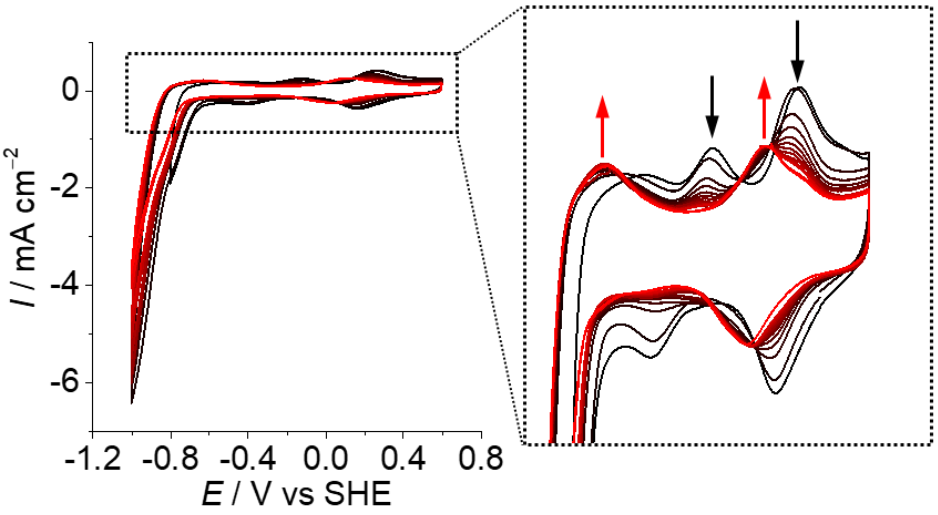

*Figure S28: CV of the **CoN$_4$H-Ph$_{Pyr}$**|MWCNT modified electrode modified with 7.5 mM of Co complex in the soaking solution showing change in redox behavior consecutive to the catalysis over 120 CV cycles in $KHCO_3$ 0.5 M in CO_2 saturated electrolyte (v = 0.02 V s^{-1}, one cycle out of ten is shown for clarity).*

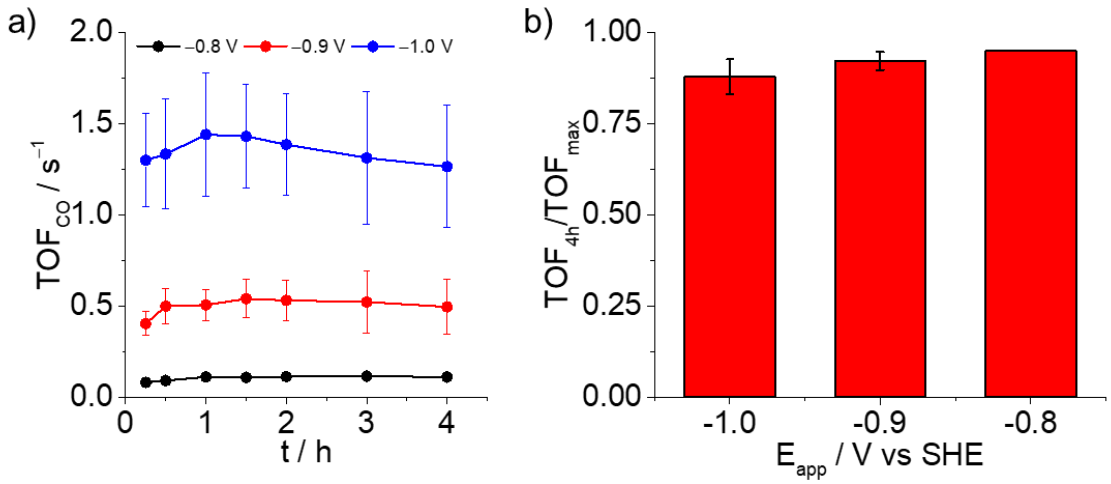

*Figure S29: a) Evolution of the TOF_{CO} (EC) overtime of **CoN$_4$H-Ph$_{Pyr}$**|MWCNT electrodes modified with 7.5 mM of Co complex in the soaking solution at different applied potential –0.8 (black dots) –0.9 (red dots) and –1.0 V vs SHE (blue dots) in 0.5 M $KHCO_3$ degassed with CO_2 (pH 7.4) b) ratio of the remaining TOF_{CO} over the maximum TOF_{CO} after 4 h of CA a various potential.*

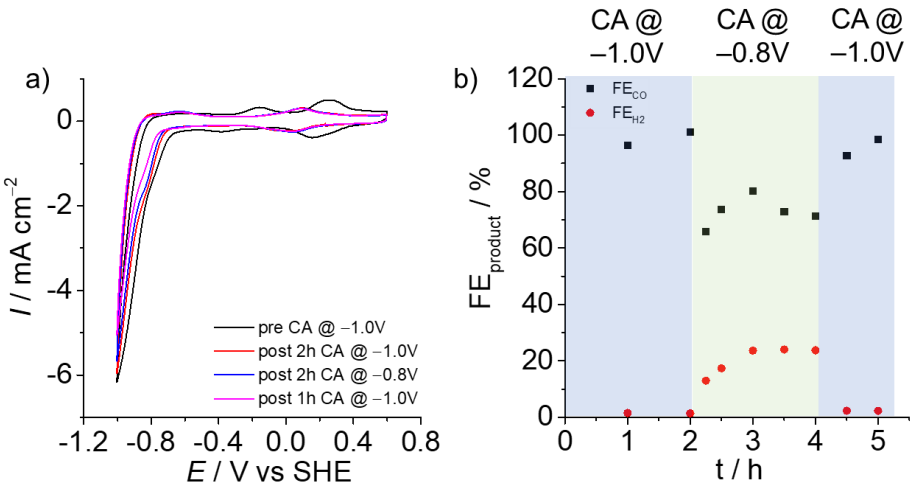

Figure S30: a) CV of the ***CoN$_4$H-Ph$_{Pyr}$****|MWCNT modified electrode modified with 7.5 mM of Co complex in the soaking solution showing the complex redox and catalytic response following CA measurements at various potentials in $KHCO_3$ 0.5 M in CO_2 saturated electrolyte (v = 0.02 V s^{-1}); b) FE for CO and H_2 during CA at different applied potential showcasing that the selectivity for CO is potential dependant rather than linked to the original or newly generated species.*

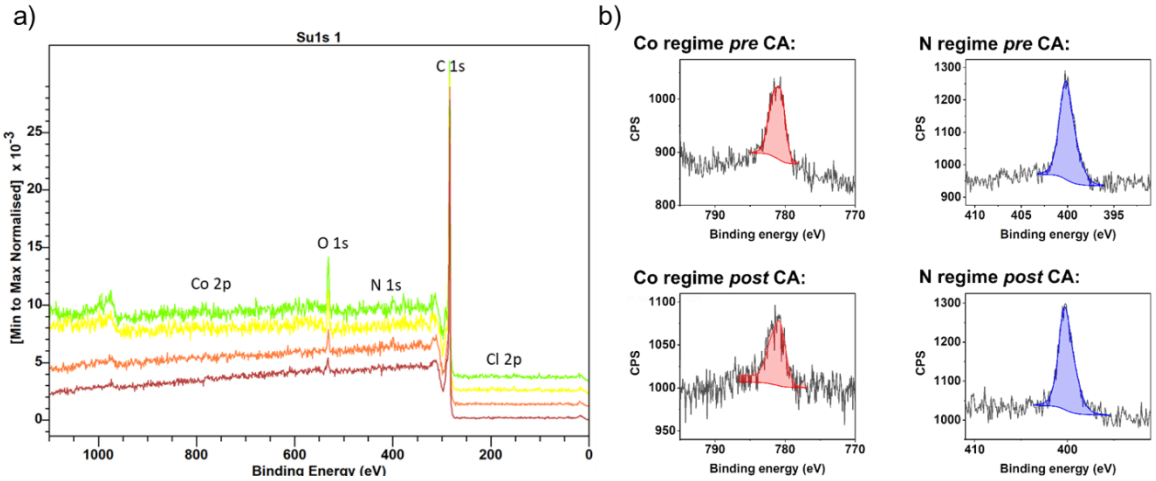

Figure S31: a) XPS survey scan of the bare MWCNT film (red trace), ***CoN$_4$H-Ph$_{Pyr}$****|MWCNT electrode modified with 7.5 mM of Co complex before (orange trace) and after CV (yellow) or CA at –1.0 V vs SHE (green trace); b) details of the Co 2p$_{3/2}$ (left) and N 1s (right) regions of the* ***CoN$_4$H-Ph$_{Pyr}$****|MWCNT electrode modified with 7.5 mM of Co complex before (top) and after (bottom) 4 h of CA at –1.0 V vs SHE in 0.5 M $KHCO_3$ degassed with CO_2 (pH 7.4).*

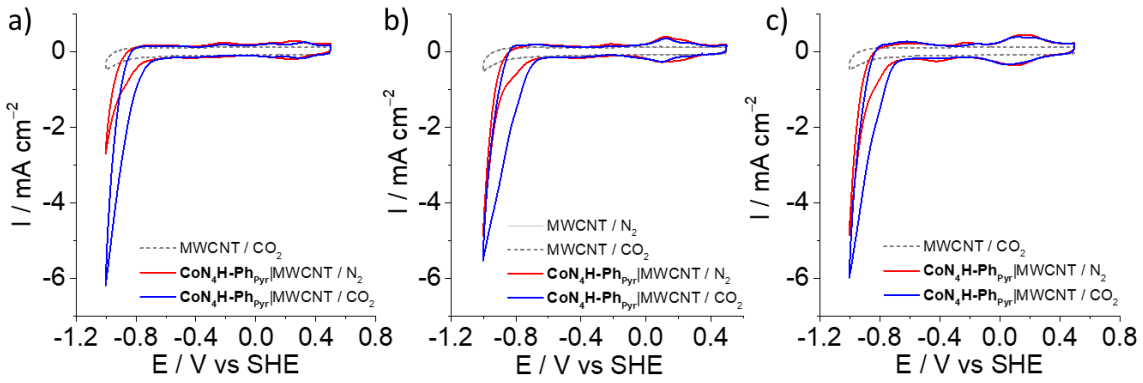

*Figure S32: CV of the **CoN_4H-Ph_{Pyr}**|MWCNT modified with a) 1.25 mM b) 7.5 mM and c) 15 mM of Co complex in the soaking solution in N_2 (red curves) and CO_2-saturated (blue curves) $KHCO_3$ 0.5 M (pH 7.4) (v = 0.02 V s^{-1}).*

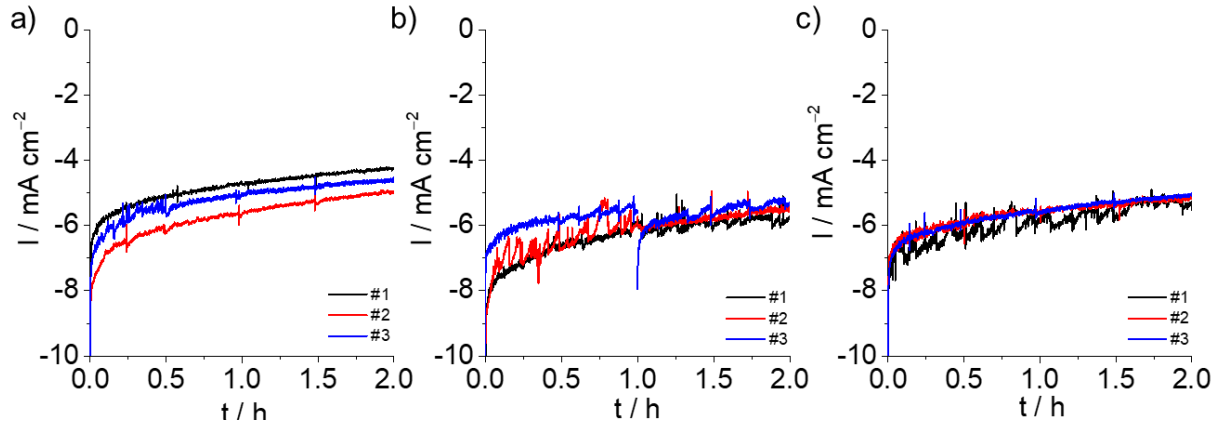

*Figure S33: Triplicated CA performed at –1.0 V vs SHE (black, red and blue curves) of **CoN_4H-Ph_{Pyr}**|MWCNT modified with a) 1.25 mM b) 7.5 mM and c) 15 mM of Co complex in the soaking solution in CO_2-saturated $KHCO_3$ 0.5 M (pH 7.4) for 2 hours.*

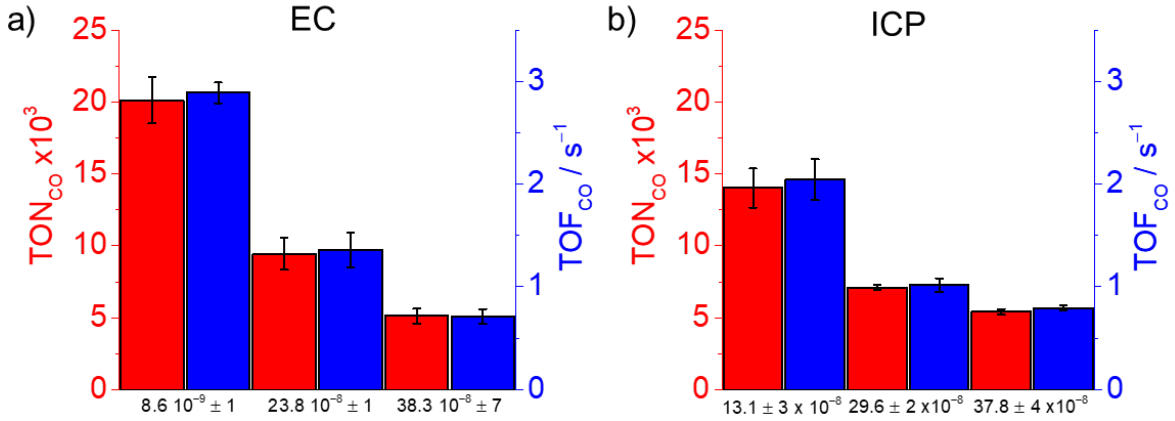

*Figure S34: TON_{CO} and TOF_{CO} **CoN_4H-Ph_{Pyr}**|MWCNT at various surface loadings calculated based on a) EC and b) ICP-OES measured catalyst loadings.*

Molecular electrode	Electrolyte	E_{onset} / V vs RHE	E_{App} / V vs RHE	J / mA cm^{-2}	FE_{CO} / %	TOF_{CO} / s^{-1}	TON_{CO} max.	stability	Ref
CoN_4H-Ph_{Pyr}|**MWCNT**	$KHCO_3$ 0.5M	–0.21	–0.56	–4.6	94	2.8	20 x10^3	2h	**This work**
CoPc|**MWCNT**	$KHCO_3$ 0.5M	–0.40	–0.63	–10	92	2.7	97 x10^3	10h	[20]
CoPc-CN|**MWCNT**	$KHCO_3$ 0.5M	–0.40	–0.63	–15	98	4.1	17.5 x10^3	1h	[20]
CoPPc|**MWCNT**	$NaHCO_3$ 0.5M	–0.30	–0.54	–12	80	0.03	76 x10^3	24h	[21]
CoPc-N^+Me_3|**MWCNT**	$NaHCO_3$ 0.5M	–0.40	–0.65	–20	91	6.8	/	10h	[22]
CoPcPPy|**PG**	NaH_2PO_4 0.1M	–0.48	–0.68	-2	89	4.8	34 x10^3	2h	[23]
Coqpy|**MWCNT**	$NaHCO_3$ 0.5M	–0.30	–0.37	–6.8	100	3.4	79.8 x10^3	6.5h	[24]
CoTPP|**MWCNT**	$KHCO_3$ 0.5M	–0.58	–0.83	–3	91	0.08	1.2 x10^3	4h	[25]
CoCPY|**MWCNT**	$KHCO_3$ 0.1M	–0.35	–0.60	–5.2	91	4.8	24 x10^3	1.4h	[26]
FeTPP-Pyr|**MWCNT**	$NaHCO_3$ 0.5M	–0.59	–0.60	–0.4	96	0.04	0.4 x10^3	3h	[27]
FeTPP-Ur|**MWCNT**	$NaHCO_3$ 0.1M	–0.4	–0.78	–1.6	90	21	151 x10^3	2h	[28]
MnPyr|**MWCNT**	$KHCO_3$ 0.5M	–0.47	–0.66	–0.5	34	0.05	1.5 x10^3	8h	[29]
MnBpy-COF|**MWCNT**	$NaHCO_3$ 0.5M	–0.30	–0.66	–15	55	0.22	6.4 x10^3	8h	[30]
MnBpy|**MWCNT**	$KHCO_3$ 0.5M	–0.39	–0.76	–13	68	/	/	/	[31]
NiCyclamPyr|**MWCNT**	$KHCO_3$ 0.1M	–0.52	–0.8	–2.6	53	/	/	4h	[32]

Table S6: Comparison of some key metrics of noble metal-free molecular cathodes for aqueous CO_2 reduction.

References

(1) Varma, S.; Castillo, C. E.; Stoll, T.; Fortage, J.; Blackman, A. G.; Molton, F.; Deronzier, A.; Collomb, M.-N. Efficient Photocatalytic Hydrogen Production in Water Using a Cobalt(III) Tetraaza-Macrocyclic Catalyst: Electrochemical Generation of the Low-Valent Co(I) Species and Its Reactivity toward Proton Reduction. *Phys. Chem. Chem. Phys.* **2013**, *15* (40), 17544–17552. https://doi.org/10.1039/C3CP52641K.

(2) Zaragoza-Galán, G.; Fowler, M. A.; Duhamel, J.; Rein, R.; Solladié, N.; Rivera, E. Synthesis and Characterization of Novel Pyrene-Dendronized Porphyrins Exhibiting Efficient Fluorescence Resonance Energy Transfer: Optical and Photophysical Properties. *Langmuir* **2012**, *28* (30), 11195–11205. https://doi.org/10.1021/la301284v.

(3) Proux, O.; Biquard, X.; Lahera, E.; Menthonnex, J.-J.; Prat, A.; Ulrich, O.; Soldo, Y.; Trévisson, P.; Kapoujyan, G.; Perroux, G.; Taunier, P.; Grand, D.; Jeantet, P.; Deleglise, M.; Roux, J.-P.; Hazemann, J.-L. FAME: A New Beamline for x-Ray Absorption Investigations of Very-Diluted Systems of Environmental, Material and Biological Interests. *Phys. Scr.* **2005**, *2005* (T115), 970. https://doi.org/10.1238/Physica.Topical.115a00970.

(4) Proux, O.; Nassif, V.; Prat, A.; Ulrich, O.; Lahera, E.; Biquard, X.; Menthonnex, J.-J.; Hazemann, J.-L. Feedback System of a Liquid-Nitrogen-Cooled Double-Crystal Monochromator: Design and Performances. *J Synchrotron Rad* **2006**, *13* (1), 59–68. https://doi.org/10.1107/S0909049505037441.

(5) Kieffer, I.; Testemale, D. SSHADE/FAME: "French Absorption Spectroscopy Beamline in Material and Environmental Science" Database Service. **2017**. https://doi.org/10.26302/SSHADE/FAME.

(6) Vichery, C.; Maurin, I.; Proux, O.; Kieffer, I.; Hazemann, J.-L.; Cortès, R.; Boilot, J.-P.; Gacoin, T. Introduction of Cobalt Ions in γ-Fe2O3 Nanoparticles by Direct Coprecipitation or Postsynthesis Adsorption: Dopant Localization and Magnetic Anisotropy. *J. Phys. Chem. C* **2013**, *117* (38), 19672–19683. https://doi.org/10.1021/jp405450p.

(7) Ravel, B.; Newville, M. ATHENA, ARTEMIS, HEPHAESTUS: Data Analysis for X-Ray Absorption Spectroscopy Using IFEFFIT. *J Synchrotron Rad* **2005**, *12* (4), 537–541. https://doi.org/10.1107/S0909049505012719.

(8) Rehr, J. J.; Kas, J. J.; Prange, M. P.; Sorini, A. P.; Takimoto, Y.; Vila, F. Ab Initio Theory and Calculations of X-Ray Spectra. *Comptes Rendus Physique* **2009**, *10* (6), 548–559. https://doi.org/10.1016/j.crhy.2008.08.004.

(9) Groom, C. R.; Bruno, I. J.; Lightfoot, M. P.; Ward, S. C. The Cambridge Structural Database. *Acta Cryst B* **2016**, *72* (2), 171–179. https://doi.org/10.1107/S2052520616003954.

(10) Moonshiram, D.; Gimbert-Suriñach, C.; Guda, A.; Picon, A.; Lehmann, C. S.; Zhang, X.; Doumy, G.; March, A. M.; Benet-Buchholz, J.; Soldatov, A.; Llobet, A.; Southworth, S. H. Tracking the Structural and Electronic Configurations of a Cobalt Proton Reduction Catalyst in Water. *J. Am. Chem. Soc.* **2016**, *138* (33), 10586–10596. https://doi.org/10.1021/jacs.6b05680.

(11) Velasco, L.; Liu, C.; Zhang, X.; Grau, S.; Gil-Sepulcre, M.; Gimbert-Suriñach, C.; Picón, A.; Llobet, A.; DeBeer, S.; Moonshiram, D. Mapping the Ultrafast Mechanistic Pathways of Co Photocatalysts in Pure Water through Time-Resolved X-Ray Spectroscopy. *ChemSusChem* **2023**, *16* (21), e202300719. https://doi.org/10.1002/cssc.202300719.

(12) Westre, T. E.; Kennepohl, P.; DeWitt, J. G.; Hedman, B.; Hodgson, K. O.; Solomon, E. I. A Multiplet Analysis of Fe K-Edge 1s → 3d Pre-Edge Features of Iron Complexes. *J. Am. Chem. Soc.* **1997**, *119* (27), 6297–6314. https://doi.org/10.1021/ja964352a.

(13) Liu, Y.; Deb, A.; Leung, K. Y.; Nie, W.; Dean, W. S.; Penner-Hahn, J. E.; McCrory, C. C. L. Determining the Coordination Environment and Electronic Structure of Polymer-Encapsulated Cobalt Phthalocyanine under Electrocatalytic CO2 Reduction Conditions Using in Situ X-Ray Absorption Spectroscopy. *Dalton Trans.* **2020**, *49* (45), 16329–16339. https://doi.org/10.1039/D0DT01288B.

(14) Hu, W.; Wang, D.; Ma, Q.; Reinhart, B. J.; Zhang, X.; Huang, J. The Impact of Axial Ligation on the Excited State Dynamics of Cobalt(II) Phthalocyanine. *Journal of Photochemistry and Photobiology* **2022**, *11*, 100132. https://doi.org/10.1016/j.jpap.2022.100132.
(15) Dau, H.; Liebisch, P.; Haumann, M. X-Ray Absorption Spectroscopy to Analyze Nuclear Geometry and Electronic Structure of Biological Metal Centers—Potential and Questions Examined with Special Focus on the Tetra-Nuclear Manganese Complex of Oxygenic Photosynthesis. *Anal Bioanal Chem* **2003**, *376* (5), 562–583. https://doi.org/10.1007/s00216-003-1982-2.
(16) Pasquini, C.; Liu, S.; Chernev, P.; Gonzalez-Flores, D.; Mohammadi, M. R.; Kubella, P.; Jiang, S.; Loos, S.; Klingan, K.; Sikolenko, V.; Mebs, S.; Haumann, M.; Beyer, P.; D'Amario, L.; Smith, R. D. L.; Zaharieva, I.; Dau, H. Operando Tracking of Oxidation-State Changes by Coupling Electrochemistry with Time-Resolved X-Ray Absorption Spectroscopy Demonstrated for Water Oxidation by a Cobalt-Based Catalyst Film. *Anal Bioanal Chem* **2021**, *413* (21), 5395–5408. https://doi.org/10.1007/s00216-021-03515-0.
(17) Leung, C.-F.; Chen, Y.-Z.; Yu, H.-Q.; Yiu, S.-M.; Ko, C.-C.; Lau, T.-C. Electro- and Photocatalytic Hydrogen Generation in Acetonitrile and Aqueous Solutions by a Cobalt Macrocyclic Schiff-Base Complex. *International Journal of Hydrogen Energy* **2011**, *36* (18), 11640–11645. https://doi.org/10.1016/j.ijhydene.2011.06.062.
(18) Laviron, E. General Expression of the Linear Potential Sweep Voltammogram in the Case of Diffusionless Electrochemical Systems. *Journal of Electroanalytical Chemistry and Interfacial Electrochemistry* **1979**, *101* (1), 19–28. https://doi.org/10.1016/S0022-0728(79)80075-3.
(19) Hanna, C. M.; Sanborn, C. D.; Ardo, S.; Yang, J. Y. Interfacial Electron Transfer of Ferrocene Immobilized onto Indium Tin Oxide through Covalent and Noncovalent Interactions. *ACS Appl. Mater. Interfaces* **2018**, *10* (15), 13211–13217. https://doi.org/10.1021/acsami.8b01219.
(20) Zhang, X.; Wu, Z.; Zhang, X.; Li, L.; Li, Y.; Xu, H.; Li, X.; Yu, X.; Zhang, Z.; Liang, Y.; Wang, H. Highly Selective and Active CO2 Reduction Electrocatalysts Based on Cobalt Phthalocyanine/Carbon Nanotube Hybrid Structures. *Nature Communications* **2017**, *8*, 14675. https://doi.org/10.1038/ncomms14675.
(21) Han, N.; Wang, Y.; Ma, L.; Wen, J.; Li, J.; Zheng, H.; Nie, K.; Wang, X.; Zhao, F.; Li, Y.; Fan, J.; Zhong, J.; Wu, T.; Miller, D. J.; Lu, J.; Lee, S.-T.; Li, Y. Supported Cobalt Polyphthalocyanine for High-Performance Electrocatalytic CO2 Reduction. *Chem* **2017**, *3* (4), 652–664. https://doi.org/10.1016/j.chempr.2017.08.002.
(22) Wang, M.; Torbensen, K.; Salvatore, D.; Ren, S.; Joulié, D.; Dumoulin, F.; Mendoza, D.; Lassalle-Kaiser, B.; Işci, U.; Berlinguette, C. P.; Robert, M. CO 2 Electrochemical Catalytic Reduction with a Highly Active Cobalt Phthalocyanine. *Nature Communications* **2019**, *10* (1), 3602. https://doi.org/10.1038/s41467-019-11542-w.
(23) Kramer, W. W.; McCrory, C. C. L. Polymer Coordination Promotes Selective CO2 Reduction by Cobalt Phthalocyanine. *Chem. Sci.* **2016**, *7* (4), 2506–2515. https://doi.org/10.1039/C5SC04015A.
(24) Wang, M.; Chen, L.; Lau, T.-C.; Robert, M. A Hybrid Co Quaterpyridine Complex/Carbon Nanotube Catalytic Material for CO2 Reduction in Water. *Angewandte Chemie International Edition* **2018**, *57* (26), 7769–7773. https://doi.org/10.1002/anie.201802792.
(25) Hu, X.-M.; Rønne, M. H.; Pedersen, S. U.; Skrydstrup, T.; Daasbjerg, K. Enhanced Catalytic Activity of Cobalt Porphyrin in CO2 Electroreduction upon Immobilization on Carbon Materials. *Angewandte Chemie International Edition* **2017**, *56* (23), 6468–6472. https://doi.org/10.1002/anie.201701104.
(26) Sun, L.; Huang, Z.; Reddu, V.; Su, T.; Fisher, A. C.; Wang, X. A Planar, Conjugated N4-Macrocyclic Cobalt Complex for Heterogeneous Electrocatalytic CO2 Reduction with High Activity. *Angewandte Chemie International Edition* **2020**, *59* (39), 17104–17109. https://doi.org/10.1002/anie.202007445.

(27) Maurin, A.; Robert, M. Noncovalent Immobilization of a Molecular Iron-Based Electrocatalyst on Carbon Electrodes for Selective, Efficient CO2-to-CO Conversion in Water. *J. Am. Chem. Soc.* **2016**, *138* (8), 2492–2495. https://doi.org/10.1021/jacs.5b12652.
(28) Zhang, C.; Dragoe, D.; Brisset, F.; Boitrel, B.; Lassalle-Kaiser, B.; Leibl, W.; Halime, Z.; Aukauloo, A. Second-Sphere Hydrogen-Bonding Enhances Heterogeneous Electrocatalytic CO2 to CO Reduction by Iron Porphyrins in Water. *Green Chem.* **2021**, *23* (22), 8979–8987. https://doi.org/10.1039/D1GC02546E.
(29) Reuillard, B.; Ly, K. H.; Rosser, T. E.; Kuehnel, M. F.; Zebger, I.; Reisner, E. Tuning Product Selectivity for Aqueous CO2 Reduction with a Mn(Bipyridine)-Pyrene Catalyst Immobilized on a Carbon Nanotube Electrode. *J. Am. Chem. Soc.* **2017**, *139* (41), 14425–14435. https://doi.org/10.1021/jacs.7b06269.
(30) Dubed Bandomo, G. C.; Mondal, S. S.; Franco, F.; Bucci, A.; Martin-Diaconescu, V.; Ortuño, M. A.; van Langevelde, P. H.; Shafir, A.; López, N.; Lloret-Fillol, J. Mechanically Constrained Catalytic Mn(CO)3Br Single Sites in a Two-Dimensional Covalent Organic Framework for CO2 Electroreduction in H2O. *ACS Catal.* **2021**, 7210–7222. https://doi.org/10.1021/acscatal.1c00314.
(31) DeLuca, E. E.; Chan, T.; Taylor, J. M.; Lee, B.; Prabhakar, R. R.; Kubiak, C. P. Steric Effects on CO2 Reduction with Substituted Mn(Bpy)(CO)3X-Type Catalysts on Multiwalled Carbon Nanotubes Reveal Critical Mechanistic Details. *ACS Catal.* **2024**, *14* (3), 2071–2083. https://doi.org/10.1021/acscatal.3c05771.
(32) Pugliese, S.; Huan, N. T.; Solé-Daura, A.; Li, Y.; Rivera de la Cruz, J.-G.; Forte, J.; Zanna, S.; Krief, A.; Su, B.-L.; Fontecave, M. CO2 Electroreduction in Water with a Heterogenized C-Substituted Nickel Cyclam Catalyst. *Inorg. Chem.* **2022**, *61* (40), 15841–15852. https://doi.org/10.1021/acs.inorgchem.2c01645.